THE ACID TEST: CALCIUM SIGNALING IN THE SKELETOGENIC LAYER OF REEF-BUILDING CORAL

By

Aaron M. Florn

A THESIS

Submitted to
Michigan State University
in partial fulfillment of the requirements
for the degree of

Zoology - Master of Science

2014

ABSTRACT

THE ACID TEST: CALCIUM SIGNALING IN THE SKELETOGENIC LAYER OF REEF-BUILDING CORAL

By

Aaron M. Florn

Since the Industrial Revolution, carbon dioxide (CO₂) emissions have increased more than 40%. This increased atmospheric CO₂ drives ocean acidification and has potentially serious consequences for all marine life, especially calcifying organisms. The specific goal of this thesis was to study calcium homeostasis and signaling dynamics within the skeletogenic tissue layers (calicodermal cells) of two coral species (Pavona maldivensis and Porites rus) at three pH treatments corresponding to present-future ocean acidification levels. Confocal microscopy techniques were used to analyze in vivo calcium dynamics of the calicodermal cells in Pavona maldivensis and Porites rus. The results show biological variation between the two reef-building coral species and their response to ocean acidification. Pavona maldivensis showed a significant difference (p < 0.01) in the ionomycin-induced calcium response among the pH treatments, but not among the microcolonies. Porites rus did not show a significant difference (p < 0.01) in the ionomycin-induced calcium response among the pH treatments or the microcolonies. Upon comparing the calcium response curves, the ionomycin-induced calcium response exhibited by Pavona maldivensis is phenomenologically similar to a calcium response that is commonly found in vertebrates. This well-studied phenomenon in vertebrate biology is known as storeoperated calcium entry (SOCE) and is closely associated with the endoplasmic reticulum (ER) and mitochondria-associated endoplasmic reticulum (MAM) calcium stores. This study provides insight into the preliminary steps needed to understand in vivo calcium signaling in the calicodermis of reef-building coral and the associated consequences of ocean acidification.

Copyright by AARON M. FLORN 2014

ACKNOWLEDGMENTS

Working on coral reef biology and physiology in the middle of Michigan has its complications as one can imagine. Through persistence, the determination to succeed and the support of good people I was able to hurdle the numerous obstacles I encountered. In this section I would like to expand on the people that have supported me throughout my graduate career.

My current career path started the spring of Spring of 2009 at Michigan State University. I was a sophomore in undergrad and I was attending the first lecture of Richard Hill's Environmental Physiology course. Unfortunately, Dick was unable to attend the first lecture as he was off SCUBA diving in the tropics for his research. Needless to say, this sparked my interest, as I was an avid SCUBA diver who loved the coral reef. Over the following years, Dick and I worked on a number of projects together, collaboratively taught courses together and became close friends. After being offered to pursue a master's program in Dick's lab I was able to develop and hone my skills as a researcher. I am very thankful for his aspiring guidance, invaluable constructive criticism and friendly advice over the years. As my research project was spattered with complexities I could not successfully complete my thesis without the support of my other wonderful committee members, Melinda Frame and Nathaniel Ostrom.

I would also like to extend my gratitude to a few other facility members at MSU for the tremendous impact they played in my graduate career. A very special thank you goes out to Dick and Sue Hill as they value the importance of educating the young minds that attend class. Being able to simplify complex topics takes years of practice and I thoroughly enjoyed learning

from the best. In addition to teaching, I needed space to do my research and Alex Shingleton was kind enough to offer me some in this dog eat dog world where space is a hot commodity.

Without the help of A&M Aquatics (Lansing, MI), especially William Backus, Brian Wagner, and Ryan Shelander, I would have had a coral-less research project. Since maintaining the livelihood of a research aquarium is a full time job, I would like to give a special thanks to Torrin McDonald for all his efforts throughout my master's research. I would also like to thank Kate Overly for her assistance in helping maintain my research aquarium.

Like any research, it is filled with many late nights and early mornings. Austin Dreyer and I were like two pees in a pod. Whether we were working in the lab, teaching, or just hanging out, we always enjoyed each other's company. Nick Testa and I first met when we taught Comparative Vertebrate Anatomy together. Since then, our friendship quickly grew upon the basic principles of respect, sarcasm and shenanigans. Additionally, I cannot forget my roommates Zach Truran and Mike Huerta for their support and understanding of my hectic schedule. Without the help of friends to share the good and the bad, it would have been a long dreary road. This is why I would also like to profoundly thank Carlos Anderson, Matt and Carly Houser, Neil Jacobs, Jason King, Catherine Lorenz, and Chris and Danielle Ricotta.

Last but not least, I offer my deepest and most sincere gratitude to my family.

Completing my master's degree was a laborious process, and more often than not, it kept me from my arrangements. I especially want to thank my family for understanding the last minute planning and/or cancellations that occurred on a regular basis as my research continuously went awry. Particularly, thank you to my sister Angela Cacioppo, her husband Jim Cacioppo, my grandma Donna Florn, and my granny Edith Cooke for their unwavering support and confidence in my success. And a special thank you to my parents, Mike and Ros, who were always willing

to support my endeavors. Whether it was driving up to MSU at 4 am for a broken aquarium or providing me with a delicious meal, my parents were with me every step of the way. Without you, none of this would have been possible. Thank you for your love and your profound willingness to help me succeed.

TABLE OF CONTENTS

LIST OF TABLES	
LIST OF FIGURES	X
CHAPTER 1 Coral Reef Overview	1
General Introduction	
Coral Anatomy	
Symbiodinium	
Natural Greenhouse Effect.	
Global Warming	
Climate Change: Ocean Temperature	
Climate Change: Sea Level Rise.	
Climate Change: Ocean Acidification	
Summary of Thesis Objectives	
CHAPTER 2 Methods	14
Coral Preparation and Care	
Lighting and Flow	
Heterotrophic Feeding	
Filtration	
Maintenance	17
pH Control	
Immunostaining	
Atmospheric Control of CO ₂ Concentration and pH	18
Choice of Dyes and Dye Loading	
Confocal Imaging.	
The Dynamic Changes of Intracellular Calcium in Response to Ionomycin	21
Extraction of CLSM Results and Statistical Analysis	22
CHAPTER 3 Corals on Acid: Challenging Ocean Acidification	24
Introduction	
Methods Overview	
Coral Preparation and Care	
Lighting and Flow	
Heterotrophic Feeding	
pH Control	
Immunostaining	
Confocal Imaging.	
Extraction of CLSM Results and Statistical Analysis	
Results	39

Discussion	44
Calcium in the Calicodermis	44
Vertebrate Store-Operated Calcium Entry	49
Biphasic SOCE Response in Pavona maldivensis	
Conclusion	
REFERENCES	54

LIST OF TABLES

Table 2.1 Experimental aquarium parameters. Iodine, phosphorus and strontium were measured twice weekly. Alkalinity, calcium, magnesium, nitrate, nitrite, and salinity were measured once daily. Conductivity, pH and temperature were recorded every minute via a Neptune System Apex Aquacontroller
Table 3.1 Results of a one-way ANOVA with blocking for <i>Pavona maldivensis</i> . The results show a significant difference ($p < 0.01$) in the ionomycin-induced calcium response among the pH treatments, but not among the microcolonies.
Table 3.2 Results of a Tukey's post hoc, pairwise comparison test of Pavona maldivensis at three pH treatments 40
Table 3.3 Results of a one-way ANOVA with blocking for <i>Porites rus</i> . The results did not show a significant difference ($p < 0.01$) in the ionomycin-induced calcium response among the pH treatments or the microcolonies

LIST OF FIGURES

Figure 1.1 Anatomical and histological schematic of Scleractinia. The top window of the figure illustrates the location of each histological schematic. (A) represents the an individual coral polyp, which is composed of the oral tissue. (B) represents the coenosarc, which is composed of oral and aboral tissue. This figure is from Vidal-Dupiol et al. (2009).
Figure 1.2 Radiation transmitted by the atmosphere. The atmospheric interaction of incoming solar electromagnetic radiation and Earth's outgoing thermal electromagnetic radiation (top panel). The middle panel depicts the overall absorption spectrum for Earth's atmosphere. The bottom panel shows the individual absorption spectrum for some of the major greenhouse gases, plus the Rayleigh scattering spectrum. The sun mainly emits high energy/short wavelength electromagnetic radiation in the visible spectrum (top panel). In comparison, Earth mainly emits low energy/long wavelength thermal electromagnetic radiation in the infrared spectrum (top panel). Absorption bands for the atmosphere (middle panel and bottom panel) are determined by the chemical properties of greenhouse gases: carbon dioxide, ozone, methane and nitrous oxide are some of the major greenhouse gases (bottom panel). As the concentrations of greenhouse gases increase, the incoming solar radiation is minimally affected (middle panel) because many of the greenhouse gases do not have a high energy/short wavelength absorption spectrum (bottom panel). On the contrary, Earth's outgoing thermal radiation is significantly affected (middle panel) as the concentrations of greenhouses gases increase because many of the greenhouse gases do have a low energy/long wavelength absorption spectrum (bottom panel). As a consequence of increased anthropogenic emissions, more thermal energy is trapped between Earth's surface and atmosphere, leading to global warming. This image was created by Robert A. Rohde / Global Warming Art and is available at: (http://www.globalwarmingart.com/wiki/File:Atmospheric_Transmission.png)
Figure 3.1 Schematic for ion/seawater transfer. Four hypotheses explain the transfer of ions/seawater across the calicodermis (depicted as cells above the skeleton) and into the subcalicoblastic extracellular calcifying medium (SCM), which is depicted as an open space above the skeleton. (a) A passive paracellular pathway between calicodermal cells provides ions to the SCM. (b) Bulk seawater is provided to the SCM via a paracellular pathway. (c) Ions are supplied to the SCM via an active transcellular pathway through calicodermal cells. (d) A combination of passive paracellular pathways and active transcellular pathways provides ions to the SCM. This figure is from Allemand et al. (2011).
Figure 3.2 Calcium Orange-AM and fluorescein diacetate (FDA) overlay. This image illustrates the overlay of Calcium Orange and FDA at an instantaneous point in time during the 15-minute trial of microcolony 4 at a pH of 8.15. The overlay demonstrates the response upon exciting the two fluorochromes. The red channel represents Calcium Orange-AM, indicative of free calcium in the cytosol. The green channel represents FDA, representing the calicodermal cells. Scale bar represents 100 μm

Figure 3.3 Calcium Orange-AM and fluorescein diacetate (FDA) colocalization with overlay. This image illustrates the colocalization between the two channels, illustrated by yellow, at an

instantaneous point in time during the 15-minute trial of microcolony 4 at a pH of 8.15. The red channel represents Calcium Orange-AM, indicative of free calcium in the cytosol. The green channel represents FDA, indicating the calicodermal cells. Scale bar represents 100 μm35
Figure 3.4 Calcium Orange-AM and fluorescein diacetate (FDA) colocalization. This image illustrates the colocalization between the two channels, illustrated by yellow, at an instantaneous point in time during the 15-minute trial of microcolony 4 at a pH of 8.15. In this image, the red channel (Calcium Orange-AM) and the green channel (FDA) have been removed. Scale bar represents $100~\mu m$ 36
Figure 3.5 Colocalized region of interests. This image illustrates the colocalization between the two channels (Calcium Orange-AM and fluorescein diacetate), illustrated by yellow, at an instantaneous point in time during the 15-minute trial of microcolony 4 at a pH of 8.15. Additionally, this image illustrates the regions of interest outlined by the blue areas that were later analyzed by Mander's coefficient. Scale bar represents $100 \mu m$ 37
Figure 3.6 Colocalized Region of Interests with dual channel overlay. This image illustrates the regions of interest that were overlaid upon the original dual channel image. The red channel represents Calcium Orange-AM, indicative of free calcium in the cytosol. The green channel represents FDA, indicating the calicodermal cells. The regions of interest are outlined by the blue areas and were later analyzed by Mander's coefficient. Scale bar represents $100 \mu m$ 38
Figure 3.7 The average maximum normalized intensity value ($\Delta F/F_0$, F_0 being baseline fluorescence and ΔF being fluorescence change) for microcolonies of <i>Pavona maldivensis</i> at each pH. Microcolony numbers are arbitrary and were assigned prior to the experiment. A one-way ANOVA with blocking followed by a Tukey's post hoc test yielded a significant difference ($p < 0.01$) in the average maximum normalized intensity among pH treatments (8.15 versus 7.65, $p = 0.004$ and 7.90 versus 7.65, $p = 0.004$), but not among the microcolonies ($p = 0.059$). The results demonstrate that there is a ubiquitous treatment effect across microcolonies; all microcolonies responded to the pH changes in a similar manner. Asterisk (*) denotes statistical significance between the pH treatments. Error bars represent 95% bootstrapped confidence intervals: 10,000 bootstrapped samples/replicates reconstructed the mean normalized time series response curves across all the ROIs within each microcolony
Figure 3.8 Tukey's 99% confidence intervals for <i>Pavona maldivensis</i> . This graphical representation of Tukey's post hoc test applied with a 99% confidence interval yields a pairwise difference between pH 8.15 and 7.65 ($p = 0.004$) and between pH 7.9 and 7.65 ($p = 0.004$). If the pairwise range contains zero, the difference between the pH treatments is not significant ($p < 0.01$).
Figure 3.9 The average maximum normalized intensity value ($\Delta F/F_O$, F_O being baseline fluorescence and ΔF being fluorescence change) for microcolonies of <i>Porites rus</i> at each pH. Microcolony numbers are arbitrary and were assigned prior to the experiment. A one-way ANOVA with blocking did not yield a significant difference ($p < 0.05$) in the average maximum normalized intensity among pH treatments ($p = 0.593$), or among microcolonies ($p = 0.823$). The results demonstrate that there is a ubiquitous lack of treatment effect across microcolonies;

all microcolonies responded to the pH changes in a similar manner. Error bars represent 95%	
bootstrapped confidence intervals: 10,000 bootstrapped samples/replicates reconstructed the	
mean normalized time series response curves across all the ROIs within each microcolony43	3

Figure 3.10 Ionomycin-induced calcium responses in vertebrate cells. The dynamic calcium response to ionomycin demonstrates a biphasic curve: (1) an initial transient elevation of cytosolic calcium in response to the ionomycin stimulus and (2) a sustained plateau phase that gradually tails off over time. This example illustrates one example of the functional expression of store-operated calcium entry (SOCE) in vertebrate cells. The above figure is from Elzi et al. (2001).

Figure 3.11 Average Normalized Calcium Response Curve for *Pavona maldivensis* microcolony 3: (A) The introduction of 50 μM ionomycin (at time = 40 seconds) into the environment of microcolony 3 at pH 8.15 results in a biphasic intracellular calcium response curve: (1) an initial transient elevation of cytosolic calcium within the calicodermis and (2) a sustained plateau phase that gradually decays over time. The plateau phase is entirely dependent upon extracellular calcium indicating the primary role of store-operated calcium entry (SOCE). Functional expression of SOCE represents the replenishing of MAM intracellular calcium stores upon depletion. (B) The introduction of 50μ M ionomycin into the environment of microcolony 3 (pH 7.65) results in a calcium response that is characteristic of cells in a calcium free extracellular medium: an initial transient elevation of cytosolic calcium within the calicodermis is not followed by the plateau phase. Thereby, exemplifying the effects of ocean acidification on calcium signaling responses within the calicodermis. Normalization was calculated against the baseline fluorescent intensity (Δ F/F_O, F_O being baseline fluorescence and Δ F being fluorescence change) for all microcolonies

CHAPTER 1

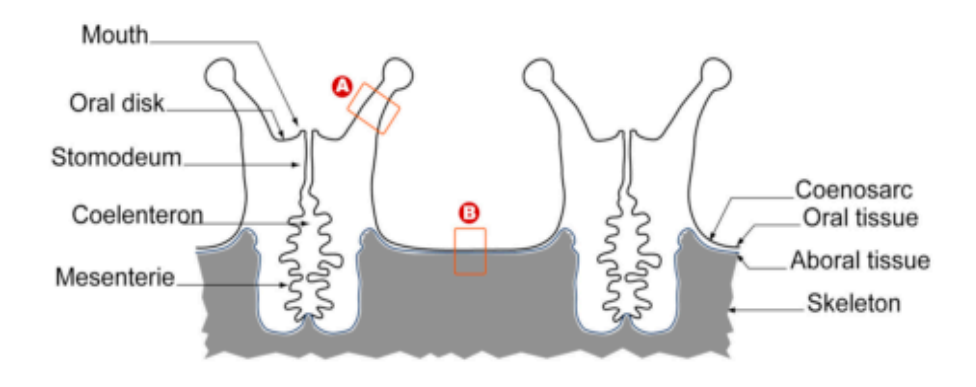
Coral Reef Overview

General Introduction

The coral reefs of the world are considered to be the rainforests of the sea owing to their natural beauty and diversity. Approximately 30% of all marine life inhabits the coral reef ecosystem, even though this ecosystem constitutes 0.1 to 0.5% of the ocean floor (Crossland et al. 1991; Spalding and Grenfell 1997; Broadgate et al. 2012; IPCC 2014). The tiny surface area of the reef ecosystem does not reflect the significant services the ecosystem provides: economic growth from local and commercial fisheries, ecotourism, and most importantly coastal protection by reducing ocean wave energy (Davis 1928; Hoegh-Guldberg 1999; Moberg and Folke 1999; Spalding et al. 2001; Donner and Potere 2007). The coral reef ecosystem may be critically important to many economies across the globe, but reefs did not take on their substantial role until recently, on a geological time scale. Some of the earliest coral ancestors first appeared as a solitary form in the fossil record more than 240 million years ago (Spalding et al. 2001; Donner and Potere 2007; Budd et al. 2010; Goatley et al. 2010; Shinzato et al. 2011). These ancient ancestors have since evolved into reef-building corals over the last 40-55 million years, leading to the formation of contemporary reefs within the past 8,000-10,000 years (Spalding et al. 2001; Donner and Potere 2007; Lough 2008; Shinzato et al. 2011; Bellwood et al. 2014). Scleractinia or reef-building coral are tiny anemone-like animals that produce a hard calcium carbonate (CaCO₃) skeleton that is responsible for the foundation of the coral reef ecosystem (Murray and Irvine 1891; Venn et al. 2012).

Coral Anatomy

Most reef-building corals are considered to be colonial organisms consisting of many polyps, except for a few species, such as fungiids, which are solitary and consist of one large polyp (Veron and Pichon 1976; Veron and Pichon 1980; Antonius 1985). A polyp is a softbodied individual coral animal (Johnston 1980; Chevalier et al. 1987; Fautin and Mariscal 1991). The polyp consists of a sac-shaped structure which is composed of several parts, notably a centralized mouth surrounded by a ring of stinging tentacles, a gastrovascular cavity that opens only at one end via the mouth, and a column as the main body (Figure 1A) (Johnston 1980; Chevalier 1987; Fautin and Mariscal 1991; Vidal-Dupiol et al. 2009; Tambutté et al. 2011). The colonial corals consist of multiple polyps that are connected by a common tissue layer, the coenosarc (Figure 1A) (Johnston 1980; Chevalier et al. 1987; Fautin and Mariscal 1991; Vidal-Dupiol et al. 2009; Tambutté et al. 2011). The tissues forming the polyp and coenosarc are comprised of the epidermis/ectoderm and gastrodermis/endoderm, shown in detail in Figure 1B. The two epithelial layers, ectoderm and endoderm, are separated by the mesoglea: a highly hydrated extracellular connective-tissue matrix primarily composed of collagen fibers (Young 1973; Bouillon and Coppois 1977; Schmid et al. 1999). The gastrovascular cavity (coelenteron) is lined by the gastrodermis/endodermal cells (Johnston 1980; Fautin and Mariscal 1991; Vidal-Dupiol et al. 2009; Tambutté et al. 2011). The skeletogenic tissue is the aboral ectoderm, often referred to as the calicoblastic ectoderm or calicodermis, which is in contact with the skeleton (Figure 1B) (Galloway et al. 2006; Musactine et al. 1997; Goldberg 2001; Vidal-Dupiol et al. 2009; Tambutté et al. 2011). The skeleton, while extracellular, is not directly exposed to the surrounding seawater because the coral polyps and coenosarc cover it (Galloway et al. 2006; Musactine et al. 1997; Goldberg 2001; Vidal-Dupiol et al. 2009; Tambutté et al. 2011). When considering all the layers, the tissue facing seaward is commonly referred to as the surface body wall/oral tissue, whereas the tissue adjacent to the skeleton is the basal body wall/aboral tissue (Galloway et al. 2006).



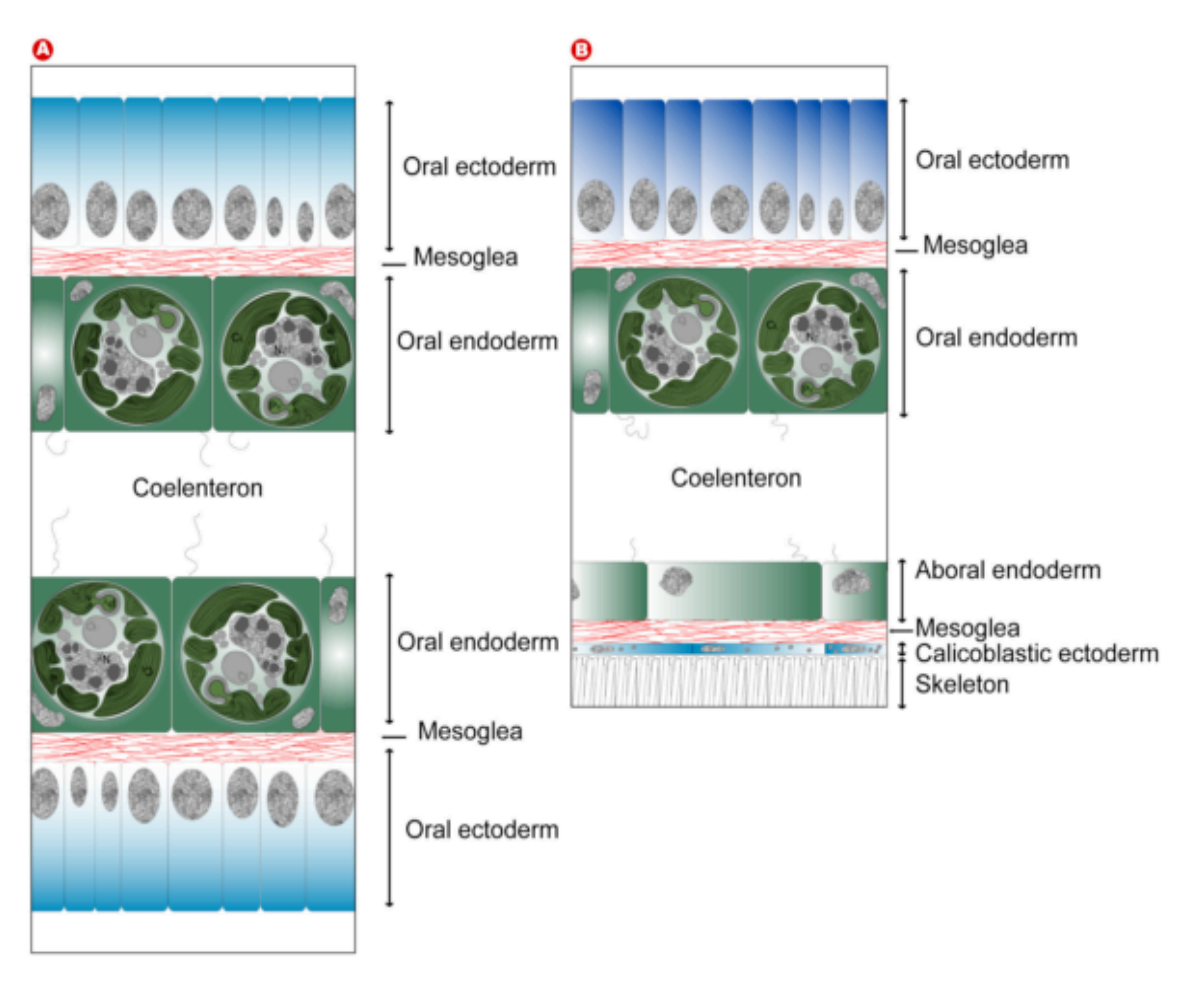


Figure 1.1 Anatomical and histological schematic of Scleractinia. The top window of the figure illustrates the location of each histological schematic. (A) represents the an individual coral polyp, which is composed of the oral tissue. (B) represents the coenosarc, which is composed of oral and aboral tissue. This figure is from Vidal-Dupiol et al. (2009).

Symbiodinium

As individual coral polyps bud from other polyps to create colonies, corals build some of the world's largest naturally occurring biological structures (Murray and Irvine 1891; Jackson 1991; Tambutté et al. 2011). These structures are formed with the symbiotic help of a dinoflagellate (*Symbiodinium sp.*), commonly referred to as zooxanthellae (Ainsworth et al., 2008; Vidal-Dupiol et al. 2009; Tambutté et al. 2011; Kaniewska et al. 2012). These zooxanthellae are found in endodermal cells, most commonly the oral endoderm (Tambutté et al. 2011).

The dependence of reef-building corals upon photosynthetic, O₂-producing organisms has its advantages and disadvantages. These photoautotrophs, using approximately 0.2% of the light energy they receive from the sun, can provide up to 95% of the energy requirements for the coral host (Muscatine 1990; Barber 2007). The supplemental energy from the zooxanthellae also allows the coral host to secrete a CaCO₃ skeleton at an increased rate (Muscatine 1990). However, environmental stressors may damage the photosynthetic machinery of the zooxanthellae; many stressors, for example, result in the overproduction of reactive oxygen species, which can cause severe cellular damage (Lesser 1996; Warner et al., 1999; Jones and Hoegh-Guldberg 2001; Wooldbridge 2013). Cellular damage can lead to zooxanthellae expulsion and the eventual breakdown of symbiosis (Wooldbridge 2013). Any process (thermal stress, ultraviolet radiation, salinity shock, etc.) by which the host coral loses zooxanthellae, or has a reduction in the photosynthetic pigment concentration, is referred to as coral bleaching (Glynn and D'Croz 1990; Hayes and Buch 1990; Jokiel and Coles 1990; Hoegh-Guldberg et al. 1999; Wooldbridge 2013). Coral bleaching plays a major role in the survival of the coral as

prolonged bleaching events may lead to the demise of individual coral polyps and eventually the coral colony.

Natural Greenhouse Effect

Earth's atmosphere contains more than 65 known greenhouse gases: water vapor, carbon dioxide (CO₂), methane (CH₄), nitrous oxide (N₂O), ozone (O₃), among others (IPCC 2014). These greenhouse gases are responsible for regulating Earth's surface temperatures (Raval and Ramanathan 1989; Ramanthan et al. 1989; Gusakova and Karlin 2014). This is achieved by the atmospheric interaction of incoming solar electromagnetic radiation (Raval and Ramanathan 1989; Ramanthan et al. 1989; Fröhlich 1991; Philipona et al. 2012) and Earth's outgoing thermal electromagnetic radiation (Figure 1.2, top panel) (Raval and Ramanathan 1989; Ramanthan et al. 1989; Ohmura et al. 1998; Philipona et al. 2001).

The sun radiates electromagnetic energy at a very wide range of wavelengths, with the radiation being strongest in the visible spectrum (0.4-0.7μm) (Ramanathan et al. 1989; Philipona et al. 2012). Solar radiation enters the atmosphere where greenhouse gases have a modest effect as the energy passes through: they reflect, refract, diffract, scatter and absorb some of the incoming solar radiation (Figure 1.2, middle panel) (Ramanathan et al. 1989; Fröhlich 1991; Ohmura et al. 1998; Philipona et al. 2012). However, most of the incoming solar radiation penetrates to Earth's surface (Ramanathan et al. 1989; Fröhlich 1991; Philipona et al. 2012).

Objects on Earth's surface then reflect, refract, diffract, scatter and absorb the incoming solar energy (Ramanathan et al. 1989; Fröhlich 1991; Ohmura et al. 1998; Philipona et al. 2012). As an object absorbs the incoming solar energy, it begins to heat up (Ramanathan et al. 1989; Taylor 1991; Philipona et al. 2012). The object will then re-radiate some of the absorbed energy

back into the atmosphere, towards outer space, as infrared radiation (Figure 1.2, top panel) (Ramanathan et al. 1989; Fröhlich 1991; Taylor 1991; Ohmura et al. 1998; Philipona et al. 2012). The chemical properties and temperature of the object that is re-radiating the electromagnetic radiation determines the rate and actual wavelength of emission (Fröhlich 1991; Ohmura et al. 1998; Philipona et al. 2012). Earth's outgoing infrared radiation will interact with greenhouse gases in the atmosphere, as these molecules have absorption properties within the infrared spectrum (Figure 1.2, middle and bottom panels) (Fröhlich 1991; Ohmura et al. 1998; Philipona et al. 2012). Similarly to the objects on Earth's surface, these greenhouse gas molecules in the atmosphere will absorb the outgoing infrared radiation and begin to heat up (Ramanathan et al. 1989; Taylor 1991; Philipona et al. 2012). The greenhouse molecules rerelease the absorbed energy in the form of heat. The radiation is emitted in all directions, meaning some of the radiation is directed back toward Earth's surface. The process of greenhouse gas molecules radiating heat back towards Earth helps to regulate Earth's ordinary surface temperature by trapping some of the outgoing thermal radiation. This supplemental heating process, attributed to greenhouse gases, is the natural greenhouse effect (Ramanathan et al. 1989; Fröhlich 1991; Ohmura et al. 1998; Philipona et al. 2012).

Global Warming

By contrast, global warming involves a small increase in average temperature (compared to historic norms) at Earth's surface. This increase is attributed to increases in the concentrations of greenhouse gases/molecules in the atmosphere, thereby amplifying the natural greenhouse effect (Ramanathan et al. 1989; Taylor 1991; Philipona et al. 2012). As anthropogenic emissions increase, the amount of heat trapped by the greenhouse gases in the atmosphere will also increase

(Figure 1.2). Since the onset of the Industrial Revolution in the mid-18th century, the concentrations of many greenhouses gases have drastically increased due to anthropogenic emissions: [N₂O] has increased 20%, [CO₂] has increased 40%, and [CH₄] has increased 150% (IPCC 2014). These particular gases are usually considered to be the gases of particular importance for the global warming underway today. Anthropogenic emissions have increased Earth's average surface temperature 0.85°C since the Industrial Revolution (IPCC 2014). As anthropogenic emissions continue to increase over the next century, the estimated average surface temperature is projected to exceed 2.0°C relative to the Industrial Revolution (IPCC 2014).

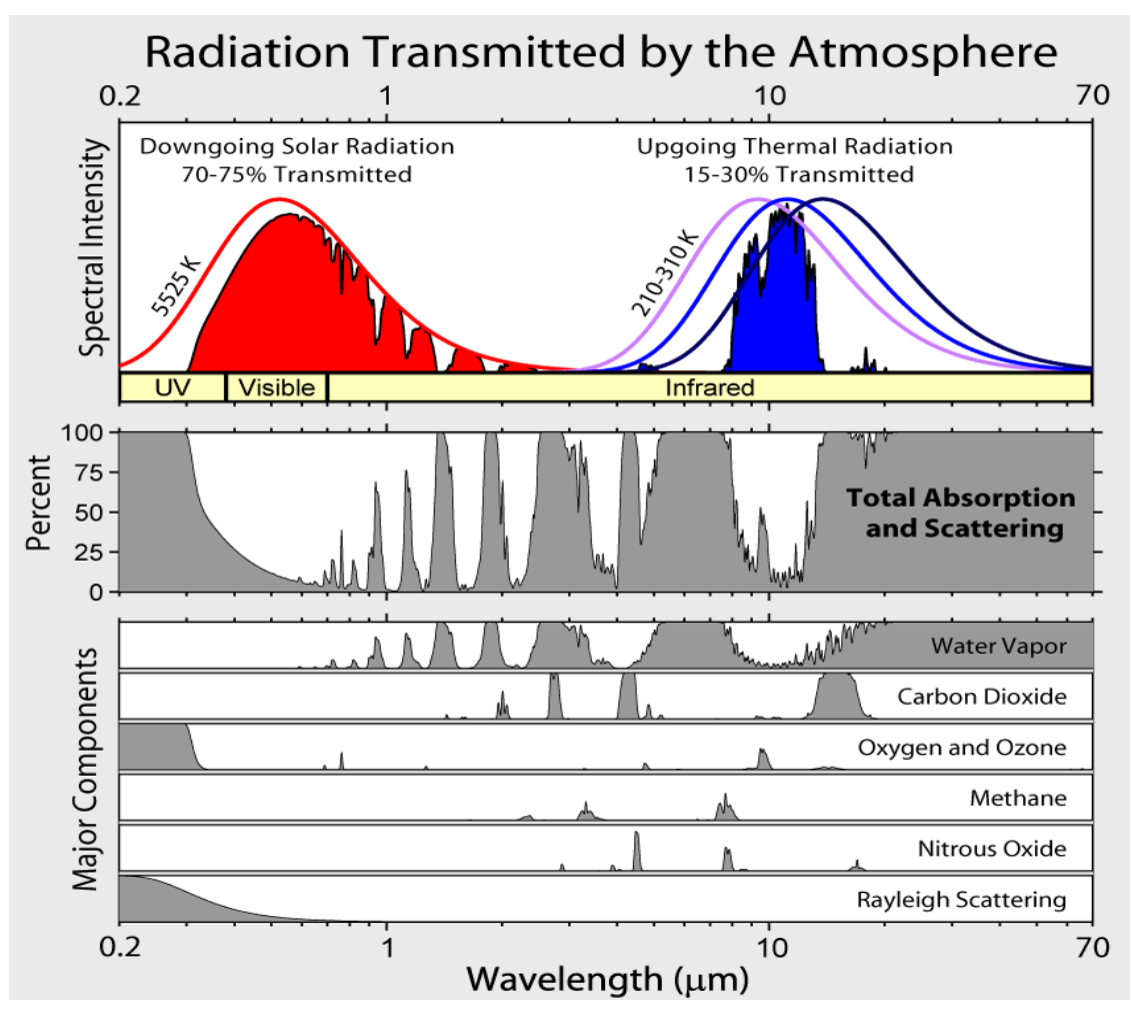


Figure 1.2 Radiation transmitted by the atmosphere. The atmospheric interaction of incoming solar electromagnetic radiation and Earth's outgoing thermal electromagnetic radiation (top panel). The middle panel depicts the overall absorption spectrum for Earth's atmosphere. The bottom panel shows the individual absorption spectrum for some of the major greenhouse gases, plus the Rayleigh scattering spectrum. The sun mainly emits high energy/short wavelength electromagnetic radiation in the visible spectrum (top panel). In comparison, Earth mainly emits low energy/long wavelength thermal electromagnetic radiation in the infrared spectrum (top panel). Absorption bands for the atmosphere (middle panel and bottom panel) are determined by the chemical properties of greenhouse gases: carbon dioxide, ozone, methane and nitrous oxide are some of the major greenhouse gases (bottom panel). As the concentrations of greenhouse gases increase, the incoming solar radiation is minimally affected (middle panel) because many of the greenhouse gases do not have a high energy/short wavelength absorption spectrum (bottom panel). On the contrary, Earth's outgoing thermal radiation is significantly affected (middle panel) as the concentrations of greenhouses gases increase because many of the greenhouse gases do have a low energy/long wavelength absorption spectrum (bottom panel). As a consequence of increased anthropogenic emissions, more thermal energy is trapped between Earth's surface and atmosphere, leading to global warming. This image was created by Robert A. Rohde / Global Warming Art and is available at: (http://www.globalwarmingart.com/wiki/File:Atmospheric Transmission.png).

Climate Change: Ocean Temperature

Earth's oceans play a major role in mitigating global warming and climate change. Records show that the oceans are responsible for absorbing approximately 90% of the total heat added via the natural greenhouse effect and global warming: 60% of the total heat is sequestered between 0-700 m and 30% of the total heat is sequestered between 700-2,000 m (Balmaseda et al. 2013; Guemas et al. 2013; IPCC 2014). As a result, sea surface temperatures (SST) increased at an average rate of 0.11°C per decade between 1971 and 2010 (IPCC 2014). By 2100, global warming models predict that the SST will increase approximately 0.06°C to 2.0°C within the first 100 m (Solomon et al. 2007; Lough, 2008; IPCC 2014). As many of the tropical reef ecosystems already function close to their upper thermal threshold, the current rate of global warming is likely to push many of the coral reef species beyond their maximum lethal tolerance level within the next century (Hoegh-Guldberg et al. 2007; Tewksbury et al. 2008; Putron et al. 2011, IPCC 2014).

Climate Change: Sea Level Rise

Sea level rise (SLR) is concurrent with global warming and increased SST. This is mainly due to the thermal expansion of seawater when heated and the melting of land-based ice (Bindoff et al. 2007; Domingues et al. 2008; Church et al. 2011; Courchamp et al. 2014). The average rate of SLR during the 20^{th} century was 1.7 ± 0.2 mm per year (Bindoff et al. 2007; Church et al. 2011; IPCC 2014). However, during the past century, sea levels have risen 3.2 ± 0.4 mm per year (IPCC 2014). By 2100, the rate of SLR is expected to increase, translating to a range of 0.52-0.98 m above present levels (Bindoff et al. 2007; Domingues et al. 2008; Church et al. 2011; Courchamp et al. 2014; IPCC 2014). Many of the models available today may

underestimate the uncertainties in thermal expansion of the oceans and ice melt and therefore, underpredict the effects of SLR (Domingues et al. 2008; Church et al. 2011).

Climate Change: Ocean Acidification

Anthropogenic CO_2 is the largest contributor to global warming and climate change (Sundquist 1993; Keeling et al. 1995; Bousquet et al. 2000; Keeling et al. 2001; Houghton 2007; Khatiwala et al. 2013). Earth's oceans play a vital role in mitigating the effects of anthropogenic emissions, especially CO_2 . Currently, Earth's oceans sequester approximately 30% of the anthropogenic CO_2 released into the atmosphere, approximately 2.2 ± 0.4 Pg (petagram = 10^{15} g) of carbon per year (Hoegh-Guldber 2007; Hönisch et al. 2012; IPCC 2014). This amount of sequestration coincides with an atmospheric $[CO_2]$ exceeding 395 parts per million (ppm), which is more than 95 ppm above the maximum values of the past 800,000 years (Hoegh-Guldberg et al. 2007; Lüthi et al. 2008; IPCC 2014).

Increased atmospheric [CO₂] drives ocean acidification, causing significant changes in the carbonate chemistry of the oceans (Hoegh-Guldberg et al. 2007; Feely et al. 2009; Venn et al. 2012; Vihtakari et al. 2013). As atmospheric CO₂ dissolves into the ocean, several reactions occur between the CO₂, water (H₂O), carbonic acid (H₂CO₃), bicarbonate ions (HCO₃⁻), and carbonate ions (CO₃²⁻). Two reactions predominate. One increases [CO₃²⁻] while reducing pH (CO₂ + H₂O \leftrightarrow H₂CO₃ \leftrightarrow H⁺ + HCO₃⁻ \leftrightarrow 2H⁺ + CO₃²⁻) (Hoegh-Guldber 2007; Feely et al. 2009; Hönisch et al. 2012; Roleda et al. 2012; IPCC 2014). The second reaction reduces [CO₃²⁻], but has no effect on pH (CO₂ + H₂O + CO₃²⁻ \leftrightarrow 2HCO₃⁻) (Hoegh-Guldberg 2007; Feely et al. 2009; Hönisch et al. 2012; Roleda et al. 2012; IPCC 2014). Together, these predominant reactions reduce the ocean's pH and [CO₃²⁻]. Corals and other marine organisms that produce CaCO₃

skeleton structures are thought to be most susceptible to ocean acidification because seawater that is undersaturated in available CO₃²⁻ ions may lead to a reduction in the calcification process required for skeleton formation (Hoegh-Guldber 2007; Feely et al. 2009; Hönisch et al. 2012; Kaniewska et al. 2012; Roleda et al. 2012; IPCC 2014).

Summary of Thesis Objectives

The specific goal of my thesis was to study calcium homeostasis dynamics in relation to ocean acidification. In particular, Ca²⁺ homeostasis dynamics within the skeletogenic tissue layers (calicodermal) of two coral species (*Pavona maldivensis* and *Porites rus*) at three pH treatments corresponding to present-future ocean acidification levels. The highest (most alkaline) experimental pH approximately corresponded to the average pH in the world's oceans during the 20th century, 8.15 (Royal Society 2005; Philip et al. 2009; IPCC 2014). The middle experimental pH approximately corresponded to some of the most acid regions of the world's ocean during the 20th century, 7.90 (Royal Society 2005; Feely et al. 2009; IPCC 2014). The lowest pH (most acidic) experimental pH approximately corresponded to the projected pH in the year 2100, 7.65 (Pecorino et al. 2013; IPCC 2014).

To study *in vivo* calcium homeostasis dynamics, I took advantage of the common pharmacological drug, ionomycin, which was used to increase cytosolic calcium concentrations. Confocal microscopy and a dual fluorochrome system allowed me to (1) identify the calicodermal cells and (2) measure free intracellular calcium within the calicodermal cytosol. Confocal time series images were acquired for each coral sample upon stimulation with ionomycin. This allowed me to observe the calcium homeostasis dynamics in response to

ionomycin. In this way, I elucidated how calcium dynamics respond to changes in seawater pH between the pH extant in the 20^{th} century and the pH expected in 2100.

Chapter 2 describes the methodology of my research, while Chapter 3 documents the importance of ocean acidification for the intracellular physiology of the *Pavona maldivensis* and *Porites rus*. My master's research in its entirety represents an important addition to the physiological understanding of ocean acidification as it effects coral reef ecosystems.

CHAPTER 2

Methods

Coral Preparation and Care

An 80-gallon seawater aquarium system was established approximately one-year prior to the introduction of the research microcolonies. To simulate a realistic coral reef environment (as close as possible), the aquarium housed a variety of common reef inhabitants, invertebrates and fish. All experimental procedures were conducted in accordance with the Institutional Animal Care and Use Committee (IACUC) at Michigan State University (MSU).

Parent colonies of *Porites rus* and *Pavona maldivensis* were propagated at A&M Aquatics (Lansing, MI). Within each species, studies were carried out on clonal subsamples ("microcolonies") cut from the parent colonies. The microcolonies were cut to approximately 5.0-cm² upward-facing surface area with an Inland (DFS-100) wet band saw (Marubini et al. 2008). Each microcolony was then placed on a glass slide in the recirculating seawater system at A&M Aquatics (Lansing, MI) so that, over the ensuing weeks, the basal portion of each newly cut coral microcolony grew out laterally across the slide as a thin sheet (Venn et al. 2011). After two months, microcolonies on slides were transported to the 80-gallon system housed at MSU, where they were introduced gradually to the new conditions by slow, drip acclimation. They were then allowed to grow out further across the glass slides under strict parameters (Table 2.1) for at least four months prior to experimentation.

Table 2.1 Experimental aquarium parameters. Iodine, phosphorus and strontium were measured twice weekly. Alkalinity, calcium, magnesium, nitrate, nitrite, and salinity were measured once daily. Conductivity, pH and temperature were recorded every minute via a Neptune System Apex Aquacontroller.

Parameter	Concentration
Total Alkalinity	187 ± 9 ppm or 10-11dKH
Total Alkallility	= 11
Calcium	$445 \pm 10 \text{ ppm}$
Conductivity	34.5 ± 0.1
Iodine	0.06 ppm
Magnesium	$1400 \pm 15 \text{ ppm}$
Nitrate	0 ppm
Nitrite	0 ppm
pH (Experiment 1)	8.15 ± 0.02
pH (Experiment 2)	7.90 ± 0.02
pH (Experiment 3)	7.65 ± 0.02
Phosphorus	$15 \pm 15 \text{ ppm}$
Salinity	$35 \pm 1 \text{ ppt}$
Strontium	$8 \pm 2 \text{ ppm}$
Temperature	25.1 ± 0.15 °C

Lighting and Flow

Environmental conditions in the 80-gallon system at MSU were maintained as consistently as possible with the environmental conditions of the parent colonies at A&M Aquatics (Lansing, MI). Microcolonies were exposed to a 12 h : 12 h photoperiod (Aquatic Life T5-HO 6-bulb with Lunar LEDs fixture (2 ATI Blue Plus, 3 ATI Aquablue Special, 1 WavePoint Red Wave, and 4 (1 Watt) Lunar LEDs) with photosynthetic active radiation (PAR) levels of $250 \pm 20 \,\mu$ mol photons m⁻² s⁻¹, measured by an Apogee Instruments Quantum Meter MQ-200, at a depth of 30 cm below the surface. Two-Ecotech Marine Vortech pumps (MP10) and a Sicce Syncra Silent 5.0 Multifunction Aquarium Pump provided randomized flow, exchanging the total water volume 25-55 times per hour.

Heterotrophic Feeding

Most reef-building corals can acquire upwards of 95% of their energy needs during the day autotrophically through their symbiotic zooxanthellae (Muscatine 1990; Barber 2007). However, heterotrophy is often important, and microcolonies were therefore target fed with food for heterotrophy three times a week during a designated cycle of one-hour feedings when coral polyps were extended (Edmunds 2011). Prior to each feeding, microcolonies acclimated to the dark for one hour inasmuch as feeding for most reef-building coral occurs at night (Barnes 1985; Heidelberg et al. 2004; Edmunds 2011). Corals were target fed a balanced diet from a cocktail solution: 6 mL of Reef Nutrition Oyster-Feast, 4 mL of Reef Nutrition Phyto-Feast, 2 mL of Reef Nutrition Roti-Feast, 2-scoops of Coral Frenzy, 0.5 mL of Brightwell Aquatics CoralAmino, and 300 mL of fresh seawater from the 80-gallon system (FSW).

Filtration

Two 100-µm felt filter socks and a Coralife 150 cone skimmer provided mechanical filtration. Seachem PhosGuard and Bulk Reef Supply (BRS) Premium ROX 0.8 Aquarium Carbon provided chemical filtration. A 15-gallon refugium contained 1-gallon of CaribSea Refugium Mineral Mud, 17.6 kg of live rock, and a variety of macro algae, providing the reef ecosystem with biological filtration.

Maintenance

All tank inhabitants were visually inspected on a daily basis. Algae were periodically removed from the glass slides and tank glass. The skimmer venturi and collection cup were cleaned three times per week. Both filter socks were replaced each week. Prior to the start of each trial, SeaChem Phosguard and BRS ROX 0.8 Carbon were replaced, a 25% water change was implemented (parameters of newly made seawater were adjusted to match the tank

parameters as needed), and Hanna Instruments Calibration Solutions were used to recalibrate pH probes.

pH Control

Experiments were conducted on microcolonies exposed to three pH environments: 8.15, 7.90, and 7.65. To achieve the desired pH for each particular trial, medical-grade CO₂ (AirGas-CDUSP50) was slowly injected into a Red Sea CO₂ Reactor incorporated in the 80-gallon aquarium system. A Neptune Systems Apex AquaController (Morgan Hill, CA 95037 USA) monitored and controlled the system. Three Neptune Systems pH probes were used as sensors; they were placed in separate areas of the 80-gallon system to ensure consistency of pH and saturation of CO₂ throughout the environment. For each pH, a 2-week acclimation period was employed. During week 1, the pH was adjusted toward the target pH by a maximum of 0.05 pH units per day; in this process, every 4-5 hours the Neptune Systems Apex Aquacontroller would slowly drop the environmental pH by 0.01 pH units. During week 2, pH was maintained at the target pH (8.15, 7.90 or 7.65). The target pH was then maintained during experimental measurements as described in the next section.

Immunostaining

*Atmospheric Control of CO*² *Concentration and pH*

For immunostaining, a small portion of the microcolony was cut (1 cm²). This small portion of the microcolony was then transferred to a small Nunc[®] Lab-Tek[®] II Chamber Slide (4 cm²/well) suitable for carrying out high-resolution imaging. Upon transferring the microcolony to the Nunc[®] Lab-Tek[®] II Chamber Slide, the microcolony was immersed in a staining cocktail solution for two hours. When microcolonies were exposed to ambient atmospheric conditions

during the incubation period, the carbonate chemistry of the cocktail solution significantly changed; therefore, the microcolonies were no longer incubating at the target pH. To overcome this issue, I custom build an atmospheric chamber. Simplistically, the atmospheric [CO₂] was used to regulate the target pH for each microcolony.

A nuAire, inc NU-701 Class III Biosafety Cabinet (C3BC) was used to tightly control atmospheric conditions during the incubation period for each microcolony. An Autopilot Greenhouse Master Controller (GMC) monitored and controlled temperature, humidity and atmospheric [CO₂] within the sealed C3BC. A Hanna Instruments combo meter (HI-98130) monitored the pH and temperature of a 50 mL sample of seawater placed immediately next to the microcolonies. A small ceramic Lasko heater (Model 5309) and homemade humidifier kept the atmosphere in the C3BC at a stable 25.1 ± 0.15 °C and 62 ± 5 % RH. A CO₂ bottle and solenoid were connected to the GMC, which injected medical grade CO₂ (AirGas-CDUSP50) into the C3BC to maintain the atmospheric [CO₂] required for each experimental pH.

Preliminary trials were conducted inside the C3BC prior to each experiment to ensure 24-hour stability of seawater parameters: alkalinity, calcium, iodine, magnesium, nitrate, nitrite, pH, phosphorus, salinity, strontium and temperature. The three pH environments, which were specifically 8.15 ± 0.03 , 7.90 ± 0.03 , and 7.65 ± 0.02 , remained stable within the C3BC at an atmospheric [CO₂] corresponding to 398 ± 6 ppm, 660 ± 10 ppm, and 1255 ± 10 ppm, respectively. A strict, stable and uniform environment inside the C3BC (atmospheric [CO₂], humidity and temperature) was produced and maintained 48 hours prior to immunostaining, assuring that seawater [CO₂] and pH were stabilized at target levels.

Choice of Dyes and Dye Loading

Analyzing intracellular calcium within the calicodermis was accomplished by a dual

fluorochrome system: (1) Calcium Orange-AM, a non-ratiometric calcium indicator that exhibits an increase in fluorescence upon binding free intracellular calcium (Takahashi et al. 1999) and (2) Fluorescein Diacetate (FDA), a cell-permeant esterase substrate that serves as a viable probe to measure enzymatic activity and cell membrane integrity in the calicodermis (Venn et al. 2011). Calcium fluorochromes, in addition to their use in the estimation of the relative intracellular calcium level, enable the spatial and temporal characterization of cytosolic calcium in living cells (Connie et al. 2005).

Coral microcolonies were removed from their slides and stained with an immunostaining cocktail. FDA and Calcium Orange-AM were prepared in stock solutions and mixed in seawater with anhydrous dimethyl sulfoxide (DMSO), with a final concentration of DMSO no greater than 0.1% v/v. The seawater was at the [CO₂] and pH appropriate for each trial (pH = 8.15, 7.90 or 7.65). Final concentrations of FDA and Calcium-Orange-AM in the solutions used to immerse microcolonies for study were 200 μ M and 40.8 μ M, respectively. Microcolonies were incubated in the atmospheric chamber for 2 hours after immersion in the immunostaining cocktail before being gently rinsed with fresh seawater. The FDA (F1301), Calcium Orange-AM (C-3015), and DMSO (D12345) were purchased from Invitrogen.

Confocal Imaging

In vivo coral microcolonies were viewed and imaged with an Olympus FluoView FV1000 Laser Scanning Confocal Microscope (Olympus America, Inc., Center Valley, PA) and Olympus FluoView FV1000 ASW software (version 3.01), referred to henceforth as CLSM. As scleractinian corals secrete a complex porous skeleton (Hughes 1987), inverted confocal microscopy was used, and images were acquired of tissue between pores and skeletal crystals in

areas of new growth. All microcolonies were imaged with a pinhole set at 1 Airy Unit using a 10x objective (Olympus UPlanSApo 10x, NA0.40) with three different filters: FDA was excited with a 488nm laser and recorded with a 510-540nm barrier filter, Calcium Orange-AM was excited with a 559nm laser and recorded with a 565-595nm barrier filter, and gray scale images were acquired with bright-field illumination.

The Dynamic Changes of Intracellular Calcium in Response to Ionomycin

Ionomycin is a cell permeable calcium ionophore that is employed to study calcium
dynamics in virtually all cell types by increasing cytosolic calcium (Morgan and Jacob 1994;
Huang and Putney 1998; Dedkova et al. 2000; Parekh and Putney 2005; Feske 2013; Müller et
al. 2013). For example, ionomycin induces a biphasic calcium response in human epithelial
cells: (1) Ionomycin evokes a calcium signaling pathway, in which calcium is released from
intracellular stores yielding a spike in cytosolic calcium and (2) store-operated calcium entry
(SOCE) mechanisms are responsible for a sustained plateau followed by a gradual decline in
cytosolic calcium (Morgan and Jacob 1994; Huang and Putney 1998; Dedkova et al. 2000;
Parkeh and Putney 2005; Feske 2013; Müller et al. 2013). Due to ionomycin's unique
properties, it is a common pharmacological tool. Since ionomycin can activate or potentially
modulate the calcium signaling pathways, the response to ionomycin amongst cell types may
significantly vary (Morgan and Jacob 1994; Dedkova et al. 2000; Müller et al. 2013).

To measure the ionomycin-induced calcium response within the calicodermis of microcolonies, the appropriate concentration of ionomycin needed to be determined. In this study, stained cells were stimulated with different concentrations of ionomycin to determine which concentration yielded a significant increase in the Calcium Orange-AM fluorescent intensity (which is a relative measurement for changes in the concentration of cytosolic calcium).

A significant increase in fluorescent intensity, indicative of a change in cytosolic calcium, was observed in microcolonies exposed to a concentration of 50 μ M ionomycin.

For each microcolony, the CLSM acquired fluorescent images at 10 second intervals over a 15-minute time period. After the first 40-seconds of imaging, 50 µM ionomycin (1 mg, purchased from Invitrogen I-24222) was introduced to induce an increase in cytosolic calcium, which was represented by the increase in fluorescent intensity of Calcium Orange-AM (Cornell-Bell et al. 1990). The CLSM generated individual and coalesced images from the three filters over time, permitting dynamic responses in intracellular calcium to be followed.

Extraction of CLSM Results and Statistical Analysis

The CLSM generated colocalized images representing the presence of the two fluorochromes at the same physical location at the same time (Dunn et al. 2011). The presence of Calcium Orange-AM and FDA in the same location were used as a benchmark for measuring cytosolic calcium (detected by Calcium Orange-AM) within the calicodermis (detected by FDA) (Venn et al. 2011). Regions of interest (ROIs) for analysis of each microcolony were then defined as being areas a high degree of overlap between FDA and Calcium Orange-AM. The Mander's overlap coefficient, a colocalization statistic representing the proportion of overlap between fluorochromes, was used to qualify all ROI's with an overlap proportion greater than 0.60. From each ROI in a particular microcolony, the CLSM generated a calcium response curve composed of the average fluorescent intensity values, measured every 10 seconds over the 15-minute CLSM study period. To standardize fluorescent intensities across all ROIs for all microcolonies, each intensity value was normalized against its own baseline fluorescence intensity (ΔF/F_O, F_O the baseline fluorescence and ΔF the fluorescence change), where the

baseline is the fluorescent intensity prior to the introduction of 50 μM ionomycin (Cornell-Bell et al. 1990). The normalized fluorescent intensity values were used to reconstruct the calcium response curve for each ROI in a particular microcolony, referred to as the normalized calcium response curve. From the normalized calcium response curves, individual time points (every 10 seconds) were averaged across all ROIs of a particular microcolony. This generated a single response curve for each microcolony, which is referred to as the average normalized calcium response curve. The maximum intensity value from each microcolonies' average normalized calcium response curve was extracted. This is referred to as the average maximum normalized intensity value. Average maximum normalized intensity values were analyzed statistically using a one-way ANOVA with blocking (R Core Team 2014). A randomized block design (RBD) was used. The defining feature of RDB is that each block is exposed to each treatment exactly once; therefore, each microcolony (block) was exposed to each pH treatment exactly once. By using microcolonies as blocks, the influence of extraneous factors was minimized.

CHAPTER 3

Corals on Acid: Challenging Ocean Acidification

Introduction

Coral reefs are responsible for creating some of the world's largest naturally occurring biological structures, owing to half the world's CaCO₃ precipitation, approximately 10 kg CaCO₃ m⁻² yr⁻¹ (Murray and Irvine 1891; Jackson 1991; Tambutté et al. 2011). For many of the reefbuilding coral species, it is known that the cell layer overlying the skeleton, termed the calicodermis, is involved in the extracellular production of CaCO₃ deposited in the skeleton (Marshall and Wright 1993; Muscatine et al. 1997; Zoccola et al. 1999; Allemand et al. 2011; Tambutté et al. 2011; Venn et al. 2012). However, almost no physiological studies have been performed *in vivo* on the calicodermis, meaning many of its physiological properties remain a biological enigma (Furla 2000a; Allemand et al. 2011; Tambutté et al. 2011).

The leading hypothesis for skeletal formation posits the delivery of calcium and inorganic carbon to the subcalicoblastic extracellular calcifying medium (SCM), thought to be the site of calcification. The SCM is a fluid medium at the interface of the calicodermis and skeleton (Barnes 1970, Barnes 1972, Allemand et al. 2011; Venn et al. 2011; Venn et al. 2012). The mechanism by which ions are supplied to the SCM is unclear, but there are four major hypotheses that have been cited in the literature. These are diagrammed in Figure 3.1 parts (a) to (d). In Figure 3.1(a), ions are provided to the SCM via a passive paracellular pathway, meaning ions passively diffuse through extracellular fluids between calicodermal cells along their natural chemical or electrochemical gradients (Kottra and Frömter 1983; Tambutté et al. 1995; Marshall 1996; Tambutté et al. 2011). Similar to the above ion pathway, Figure 3.1(b) posits that bulk seawater is provided to the SCM via a passive paracellular pathway (Karoonuthaisiri et al. 2003; Cohen and McConnaughey 2003; Erez and Braun 2007; Venn et al. 2011). In Figure 3.1(c), calcium ions are provided to the SCM via an active transcellular pathway, meaning the coral uses

energy to move ions though the calicodermal cells against their natural chemical or electrochemical gradients (Chalker and Taylor 1975; Chalker 1976; Clode and Marshall 1996; Marshall et al. 2007). In Figure 3.1(d), ions are provided to the SCM via a combination of passive paracellular pathways and active transcellular pathways (Berridge and Loschman 1972; Tambutté et al. 1996; Furla et al. 2000a; Venn et al. 2011). In addition to these pathways, researchers have speculated that mitochondria may play a large role in the biomineralization process in addition to supplying ATP, as the calicodermis contains numerous mitochondria (Muscatine et al. 1997; Furla et al. 2000a; Allemand et al. 2004; Allemand et al. 2011; Tambutté et al. 2011).

Calcium is an essential ion that is involved in a variety of biological functions (Parekh and Putney 2005; Slusarki and Pelegri 2007; Venn et al. 2011; Suganuma et al. 2012). One principal physiological function of calcium, apart from being used as a mineral deposit, is its role as an intracellular messenger (Takahashi et al. 1999; Zoccola et al. 1999; Verkhratsky and Parpura 2014). Many coral studies have focused on calcium as a mineral deposit, and how calcium is incorporated into a skeletal organic matrix (Barnes 1970; Hayes and Goreau 1977; Johnston 1980; Furla et al. 2000b; Marubini et al. 2008; Tambutté et al. 2011). However, this study takes a different approach and investigates the calcium signaling pathways within the calicodermis, pathways that may be responsible for the initiation or enhancement of the biomineralization process.

In vertebrates, much is known about calcium signaling and calcium homeostasis, which are among the key elements for biomineralization (Brini and Carafoli 2000; Hoenderop et al., 2005; Logan et al. 2014). In contrast, in corals, there is paucity of information on calcium signaling and intracellular calcium concentrations in relation to calcification, especially in the

calicodermis where intracellular calcium may regulate metamorphosis, symbiosis and skeletal deposition (Bordat et al. 2004; DeSalvo et al. 2010; Grasso et al. 2008; Reyes-Bermudez et al. 2009; DeSalvo et al. 2010; Grasso et al. 2011; Reyes-Bermudez et al. 2012). The lack of understanding of calcium metabolism in corals may be attributed to the difficulty of accessing the calicodermis, as the apical side faces the CaCO₃ skeleton and the basal side faces three other epithelial layers that separate the calicodermis from the surrounding seawater (Johnston 1980; Marshall et al. 2007; Allemand et al. 2011).

This study gained access to the calicodermis of *Porites rus* and *Pavona maldivensis* by using inverted confocal microscopy to specifically image the calicodermis between pores skeletal crystals in areas of new growth (Muscatine et al. 1997; Venn et al. 2011; Tambutté et al. 2011). A dual fluorochrome system provided insight into the physiology of the calicodermis, as the dynamics of intracellular calcium flux were measured at multiple seawater pHs ranging from the 20th-century norm to pHs characteristic of future ocean acidification.

Over the course of the present century, ocean acidification is predicted to deleteriously affect many taxa and life stages of animals, especially the reef-building corals. Ocean acidification may be attributed to the fact that Earth's oceans sequester approximately 30% of the CO₂ emitted into the atmosphere each year (Crossland et al. 1991; Spalding and Grenfell 1997; Kroeker et al. 2010; Pandolfi et al. 2011; Rodolofo-Metalpa et al. 2011; Broadgate 2012; IPCC 2014). Ocean acidification causes an alteration in the carbonate chemistry of the oceans, leading to a reduction in the ocean's pH and carbonate ion concentration ([CO₃²⁻]). Since the Industrial Revolution, ocean pH has decreased 0.1 pH units from an average pH range of 8.30 to 8.00 (Caldeira and Wickett 2003; Caldeira and Wickett 2005; Doney et al. 2009; Feely et al. 2009). Currently, the average ocean pH ranges from 8.20 to 7.90 pH units. The effects of ocean

acidification are ubiquitous, even though there are regional variations due to many extraneous factors such as biological activity, terrestrial run off, salinity, temperature, and upwelling (Zeebe 2012; Quesne and Pinnegar 2012). As anthropogenic CO₂ emissions continue to increase across the globe, the oceans are expected to decrease in pH by an additional 0.3-0.5 pH units by 2100. This is expected to lead to an average surface pH of 7.90 to 7.60 (Caldeira and Wickett 2005; Hoegh-Guldberg 2007; IPCC 2014).

In this research, calcium homeostasis in relation to ocean acidification was investigated. Specifically, calcium signaling dynamics within the calicodermis of *Pavona maldivensis* and Porites rus at three pH treatments corresponding to present-future ocean acidification levels were compared. The highest (most alkaline) experimental pH in this study approximately corresponded to the average pH in the world's oceans during the 20th century, 8.15 (Caldeira and Wickett 2003; Caldeira and Wickett 2005; Doney et al. 2009; Feely et al. 2009; Munday et al. 2009; IPCC 2014). The middle experimental pH approximately corresponded to some of the most acid regions of the world's oceans during the 20th century, 7.90 (Royal Society 2005; Feely et al. 2009; IPCC 2014). The lowest experimental pH (most acidic) approximately corresponded to the projected pH in the year 2100, 7.65 (Pecorino et al. 2013; IPCC 2014). To analyze calcium signaling dynamics within the calicodermis, this study took advantage of the fact that ionomycin activates the redistribution of intracellular calcium and calcium stores. Ionomycin was introduced to the coral microcolonies while the concentration of cytosolic calcium in calicodermal cells was monitored via confocal laser scanning microscopy. In this way, the ionomycin-induced calcium response was recorded in vivo in real time. As biological variation is likely to exist (between individuals, populations and taxa), the ionomycin-induced calcium response was investigated for two different, but related, coral species.

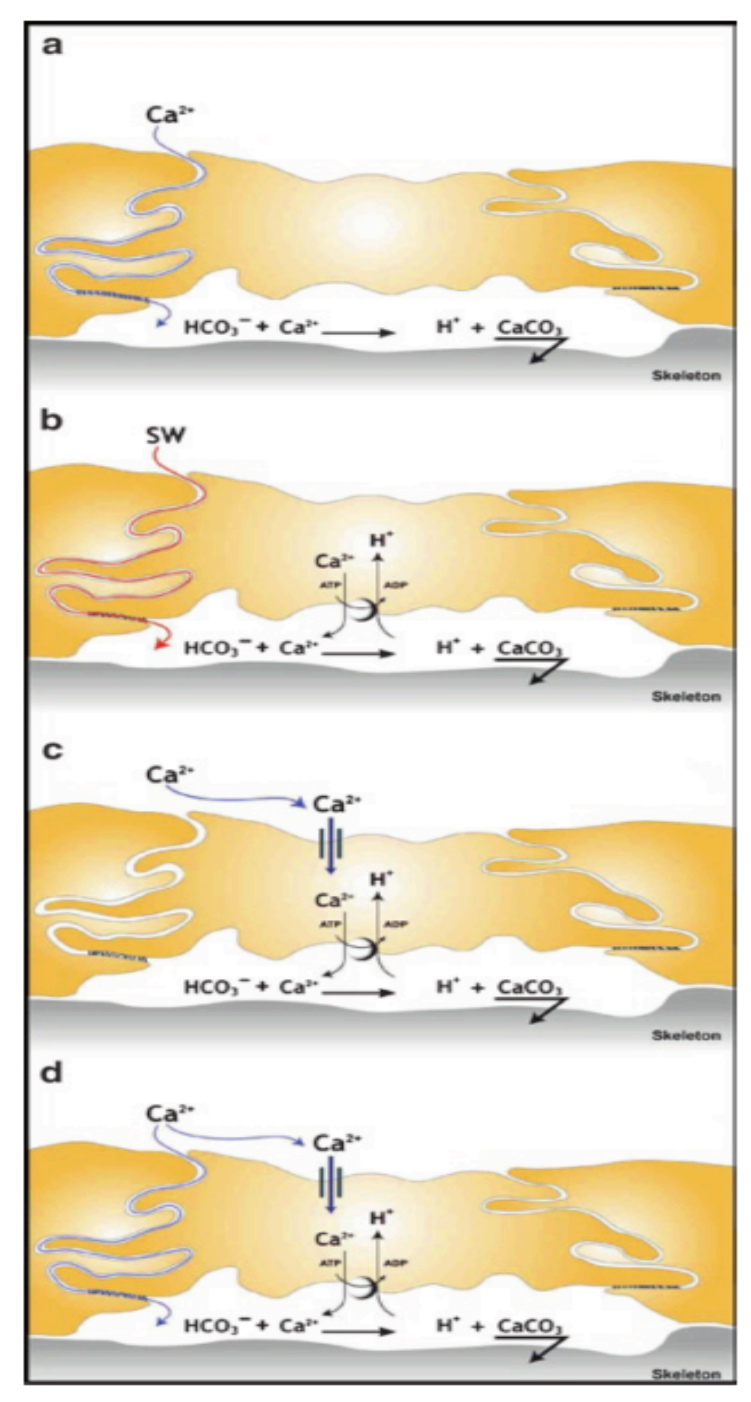


Figure 3.1 Schematic for ion/seawater transfer. Four hypotheses explain the transfer of ions/seawater across the calicodermis (depicted as cells above the skeleton) and into the subcalicoblastic extracellular calcifying medium (SCM), which is depicted as an open space above the skeleton. (a) A passive paracellular pathway between calicodermal cells provides ions to the SCM. (b) Bulk seawater is provided to the SCM via a paracellular pathway. (c) Ions are supplied to the SCM via an active transcellular pathway through calicodermal cells. (d) A combination of passive paracellular pathways and active transcellular pathways provides ions to the SCM. This figure is from Allemand et al. (2011).

Methods Overview

Coral Preparation and Care

This study investigated the *in vivo* effects of seawater acidification on intracellular calcium dynamics within the calicodermis. All experiments were conducted on microcolonies prepared from colonies of *Porites rus* and *Pavona maldivensis*. Each microcolony was cut from the parent colony and attached to a glass slide. Microcolonies grew out laterally, under tightly controlled conditions, across glass slides for at least 6 months prior to the experiments. See Chapter 2 – Coral Preparation and Care – for details.

Lighting and Flow

Microcolonies were exposed to a 12 h : 12 h photoperiod (Aquatic Life T5-HO 6-bulb with Lunar LEDs fixture (2 ATI Blue Plus, 3 ATI Aquablue Special, 1 WavePoint Red Wave, and 4 (1 Watt) Lunar LEDs) with photosynthetic active radiation (PAR) levels of $250 \pm 20 \mu mol$ photons m⁻² s⁻¹, measured by an Apogee Instruments Quantum Meter MQ-200, at a depth of 30 cm below the surface. See Chapter 2 – Lighting and Flow – for details.

Heterotrophic Feeding

Microcolonies were target fed with food for heterotrophy three times a week during a designated cycle of one-hour feedings when coral polyps were extended (Edmunds 2011). Prior to each feeding, microcolonies were acclimated to the dark for one hour inasmuch as feeding for most reef-building coral occurs at night (Barnes 1985; Heidelberg et al. 2004; Edmunds 2011). See Chapter 2 – Heterotrophic Feeding – for details.

pH Control

Each microcolony of *Pavona maldivensis* (n = 5) and *Porites rus* (n = 5) was exposed sequentially to the three pH environments already discussed: 8.15, 7.90, and 7.65. The pH was

modified and controlled by direct injection of medical grade CO₂ (AirGas-CDUSP50) into a reactor, allowing CO₂ to easily diffuse into the 80-gallon seawater aquarium where the microcolonies were maintained. For each pH, a 2-week acclimation period was employed. During week 1, the pH was adjusted toward the target pH by a maximum of 0.05 pH units per day; in this process, every 4-5 hours the Neptune Systems Apex Aquacontroller would slowly drop the environmental pH by 0.01 pH units. During week 2, pH was maintained at the target pH (8.15, 7.90 or 7.65). A Neptune Systems Apex AquaController monitored and controlled the rate of CO₂ injection into the environment using three pH probes for pH sensing. These three probes ensured consistency of pH and saturation of CO₂ throughout the environment. See Chapter 2 – pH Control – for details.

Immunostaining

The two fluorochromes, fluorescein diacetate (FDA) and Calcium Orange-AM, were dissolved in an incubation medium of fresh seawater (FSW) and dimethyl sulfoxide (DMSO), with a final concentration of DMSO no greater than 0.1% v/v. FDA and Calcium Orange-AM were added to the incubation medium at a final concentration of 200 μM and 40.8 μM, respectively. For exposure to the incubation medium, microcolonies were immersed in the medium within small, shallow study chambers that were located in a large atmospheric chamber. pH within the medium was controlled at this stage by controlling the [CO₂] in the atmosphere. Microcolonies were incubated in the medium for 2 hours before being rinsed with FSW prior to confocal imaging. See Chapter 2 – Immunostaining – for details.

Confocal Imaging

Microscope (Olympus America, Inc., Center Valley, PA) operated with Olympus FluoView

FV1000 ASW software (version 3.01), referred to henceforth as CLSM. In particular, the calicodermis was imaged between pores and skeletal crystals in areas of new growth. Images were acquired with a pinhole set at 1 Airy Unit using a 10x objective (Olympus UPlanSApo 10x, NA0.40). Three separate images – FDA excited with a 488nm laser and recorded with a 510-540nm barrier filter, Calcium Orange-AM excited with a 559nm laser and recorded with a 565-595nm barrier filter, and bright-field images – were acquired simultaneously every 10 seconds, over a 15 minute time period. After the first 40 seconds of imaging, 50 μM ionomycin was introduced to induce an increase in cytosolic calcium, which was represented by a corresponding increase in the fluorescent intensity of Calcium Orange-AM (Cornell-Bell et al. 1990). Excitement of FDA served to identify the calicodermal cells (Venn et al. 2011), whereas Calcium Orange-AM served as a relative measure for the concentration of cytosolic calcium (Figure 3.2). The CLSM generated individual and coalesced images from the three filters over time, permitting dynamic responses in intracellular calcium to be followed. See Chapter 2 – Confocal Imaging – for details.

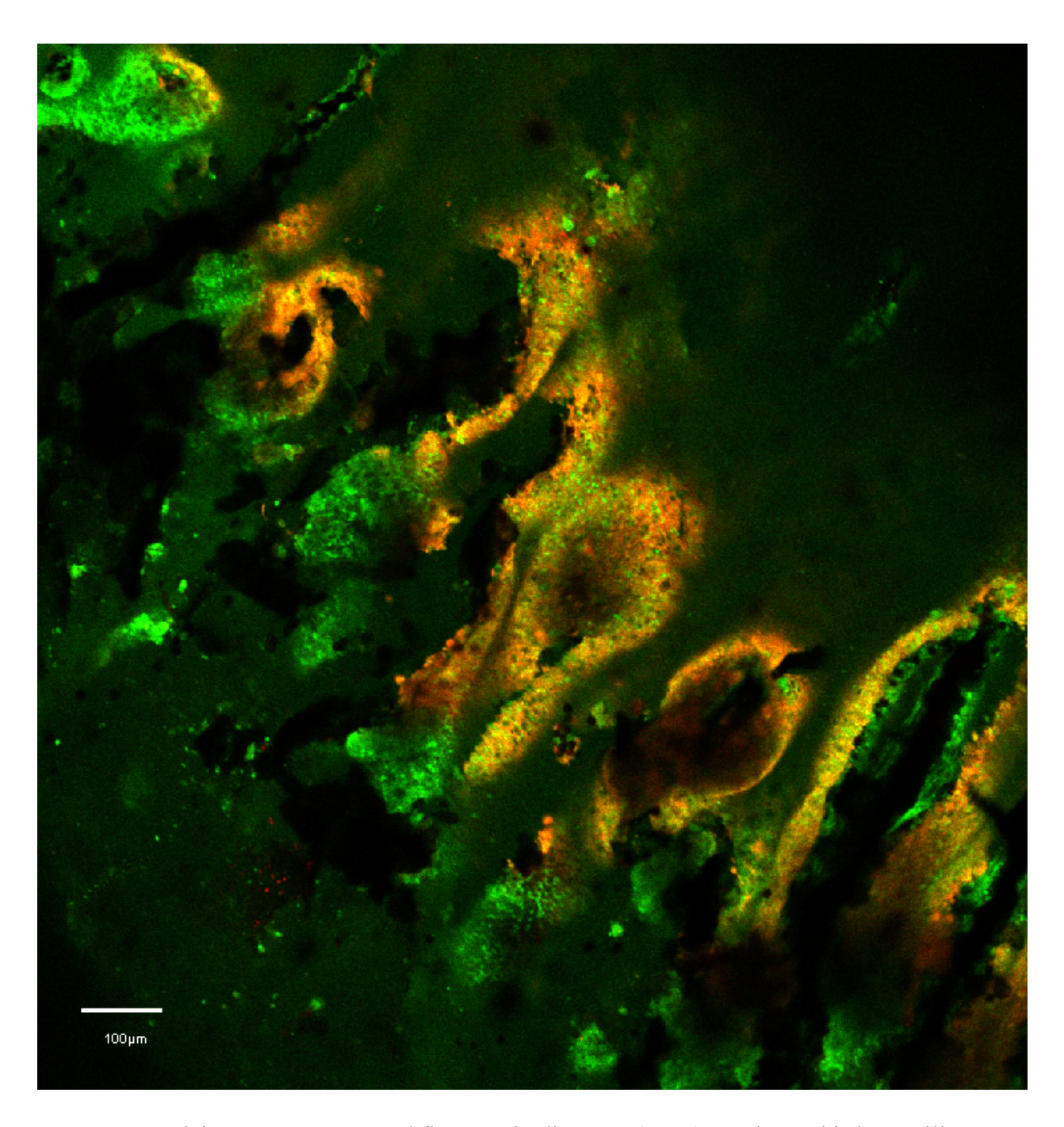


Figure 3.2 Calcium Orange-AM and fluorescein diacetate (FDA) overlay. This image illustrates the overlay of Calcium Orange and FDA at an instantaneous point in time during the 15-minute trial of microcolony 4 at a pH of 8.15. The overlay demonstrates the response upon exciting the two fluorochromes. The red channel represents Calcium Orange-AM, indicative of free calcium in the cytosol. The green channel represents FDA, representing the calicodermal cells. Scale bar represents $100~\mu m$.

Extraction of CLSM Results and Statistical Analysis

From the CLSM results, colocalized images of FDA and Calcium Orange-AM were generated, in which FDA localized the calicodermis and Calcium Orange-AM measured the concentration of cytosolic calcium within the calicodermal cells (Figure 3.3 and Figure 3.4). Regions of interest (ROIs) were generated in each image and were later analyzed using Mander's overlap coefficient (Figure 3.5 and Figure 3.6). Calcium Orange-AM intensity was then measured as a function of time over the 15 minutes of imaging for a microcolony. The intensity values from each ROI were normalized to their baseline intensity (ΔF/F_O, F_O being baseline fluorescence and ΔF being fluorescence change). Then the normalized values for all the ROIs of one microcolony were averaged. From this average response curve, the average normalized maximum intensity value was extracted. For each species, the maximum intensity values for all studied microcolonies exposed to each pH treatment was analyzed using a one-way ANOVA with blocking (R Core Team 2014), in which microcolonies were treated as blocks and the three pHs levels were treated as individual treatments. See Chapter 2 – Extraction of CLSM Results and Statistical Analysis – for details.

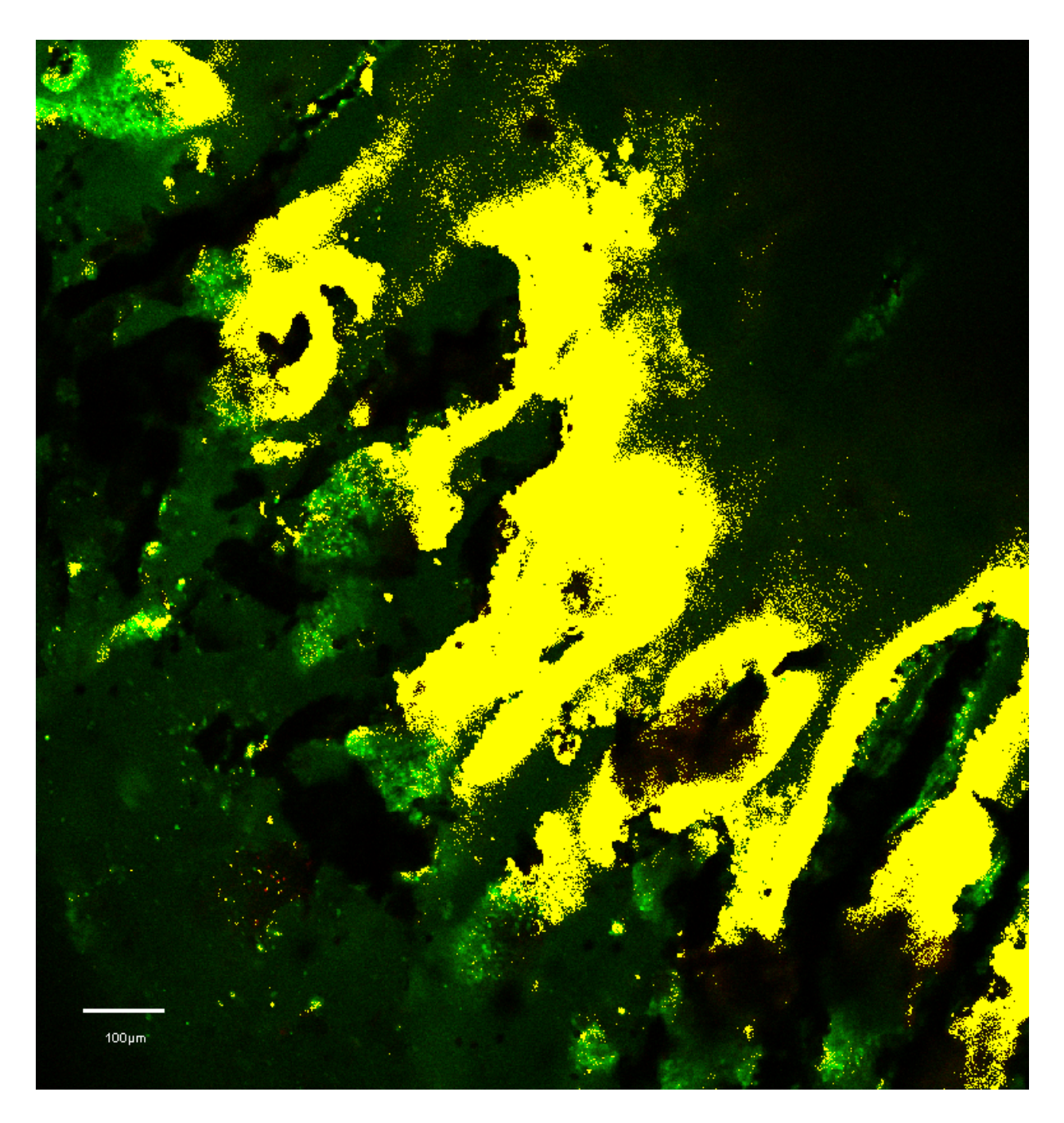


Figure 3.3 Calcium Orange-AM and fluorescein diacetate (FDA) colocalization with overlay. This image illustrates the colocalization between the two channels, illustrated by yellow, at an instantaneous point in time during the 15-minute trial of microcolony 4 at a pH of 8.15. The red channel represents Calcium Orange-AM, indicative of free calcium in the cytosol. The green channel represents FDA, indicating the calicodermal cells. Scale bar represents 100 μm.

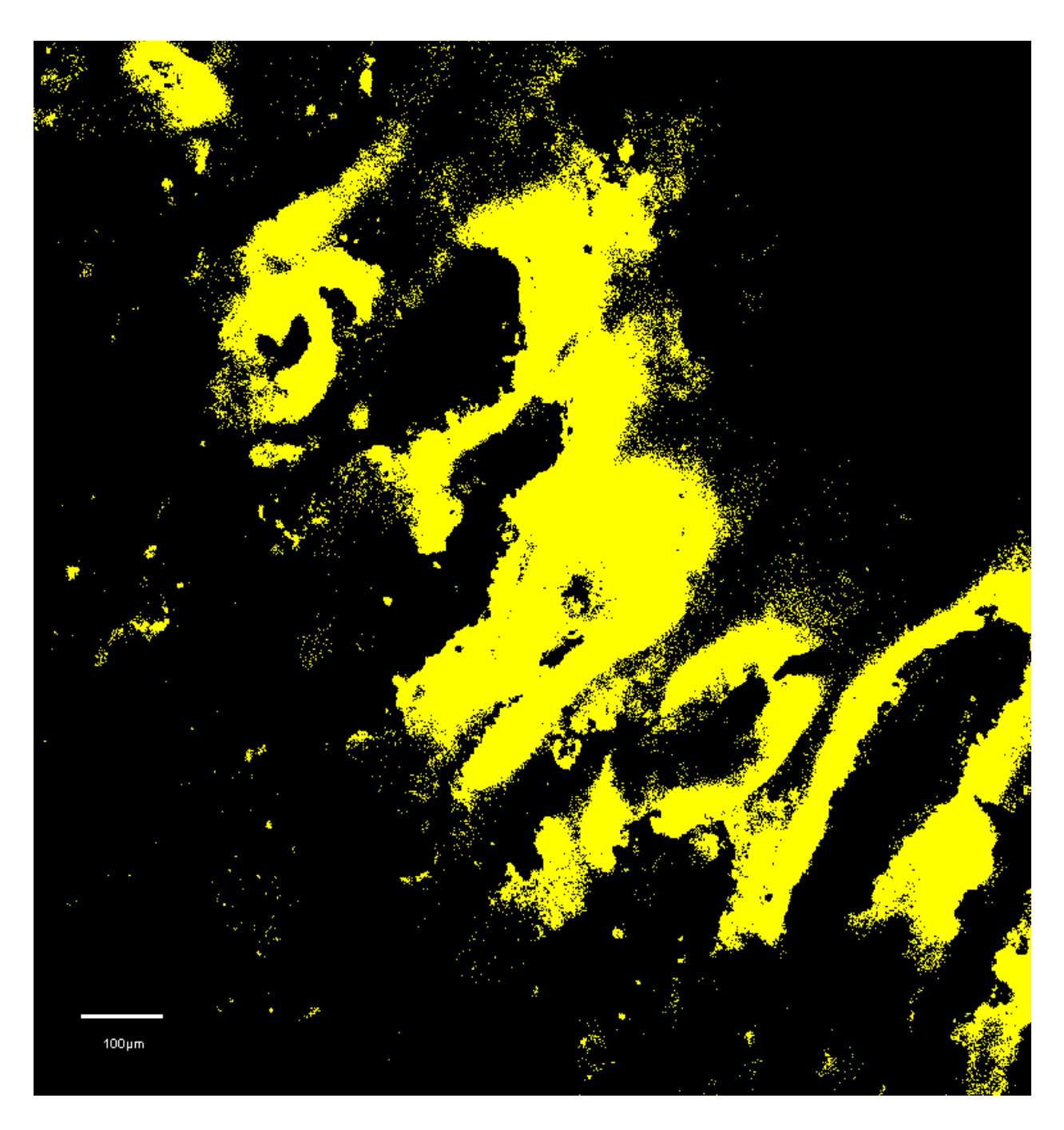


Figure 3.4 Calcium Orange-AM and fluorescein diacetate (FDA) colocalization. This image illustrates the colocalization between the two channels, illustrated by yellow, at an instantaneous point in time during the 15-minute trial of microcolony 4 at a pH of 8.15. In this image, the red channel (Calcium Orange-AM) and the green channel (FDA) have been removed. Scale bar represents $100 \ \mu m$.

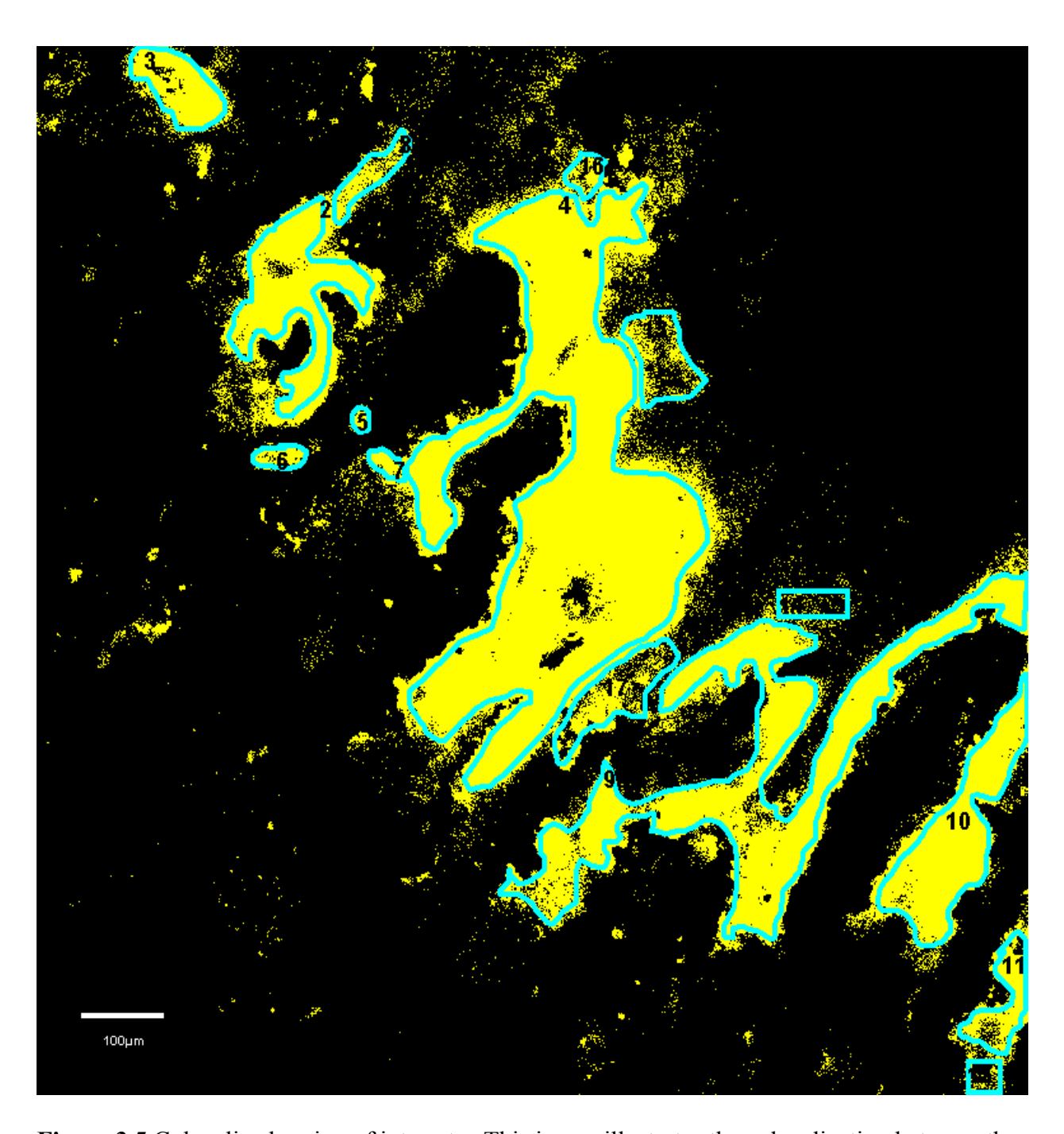


Figure 3.5 Colocalized region of interests. This image illustrates the colocalization between the two channels (Calcium Orange-AM and fluorescein diacetate), illustrated by yellow, at an instantaneous point in time during the 15-minute trial of microcolony 4 at a pH of 8.15. Additionally, this image illustrates the regions of interest outlined by the blue areas that were later analyzed by Mander's coefficient. Scale bar represents $100 \, \mu m$.

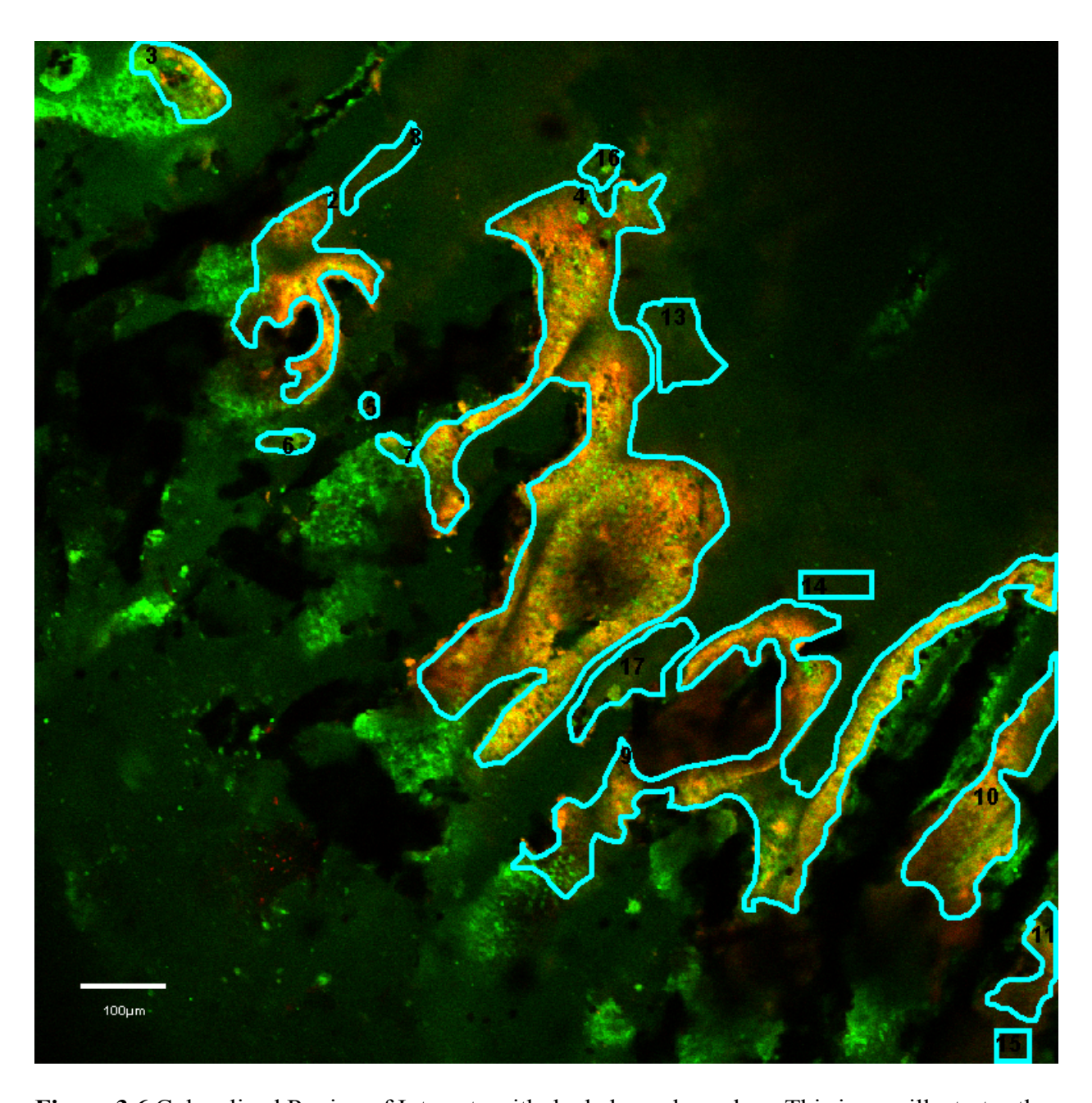


Figure 3.6 Colocalized Region of Interests with dual channel overlay. This image illustrates the regions of interest that were overlaid upon the original dual channel image. The red channel represents Calcium Orange-AM, indicative of free calcium in the cytosol. The green channel represents FDA, indicating the calicodermal cells. The regions of interest are outlined by the blue areas and were later analyzed by Mander's coefficient. Scale bar represents $100 \, \mu m$.

Results

The ionomycin-induced calcium response for *Pavona maldivensis* yielded a significant difference (p < 0.01) among the three pH treatments ($F_{2,4} = 14.783$, p = 0.002), but indicated there were no significant differences among microcolonies (blocks) ($F_{2,4} = 3.587$, p = 0.059) (Table 3.1 and Figure 3.7). A Tukey's post hoc test revealed a significant pairwise difference in the ionomycin-induced calcium response between pH 8.15 and 7.65 (p = 0.004) and between pH 7.9 and 7.65 (p = 0.004), although no significant pairwise difference between pH 8.15 and 7.9 (Table 3.2 and Figure 3.8). On the other hand, the study of *Porites rus* did not yield significant differences (p < 0.05) among the pH treatments (p = 0.593) or microcolonies (p = 0.823) (Table 3.3 and Figure 3.9). All microcolonies were monitored for four months after being exposed to the ocean acidification trials. All microcolonies successfully recuperated and continued to grow.

Table 3.1 Results of a one-way ANOVA with blocking for *Pavona maldivensis*. The results show a significant difference (p < 0.01) in the ionomycin-induced calcium response among the pH treatments, but not among the microcolonies.

	df	F Value	p Value
Microcolonies	4	3.587	0.059
pH Treatments	2	12.975	0.002

Table 3.2 Results of a Tukey's post hoc, pairwise comparison test of *Pavona maldivensis* at three pH treatments.

pH Treatments	p Value
8.15 vs 7.90	0.995
8.15 vs 7.65	0.004
7.90 vs 7.65	0.004

Table 3.3 Results of a one-way ANOVA with blocking for *Porites rus*. The results did not show a significant difference (p < 0.01) in the ionomycin-induced calcium response among the pH treatments or the microcolonies.

	df	F Value	p Value
Microcolonies	4	0.372	0.823
pH Treatments	2	0.557	0.593

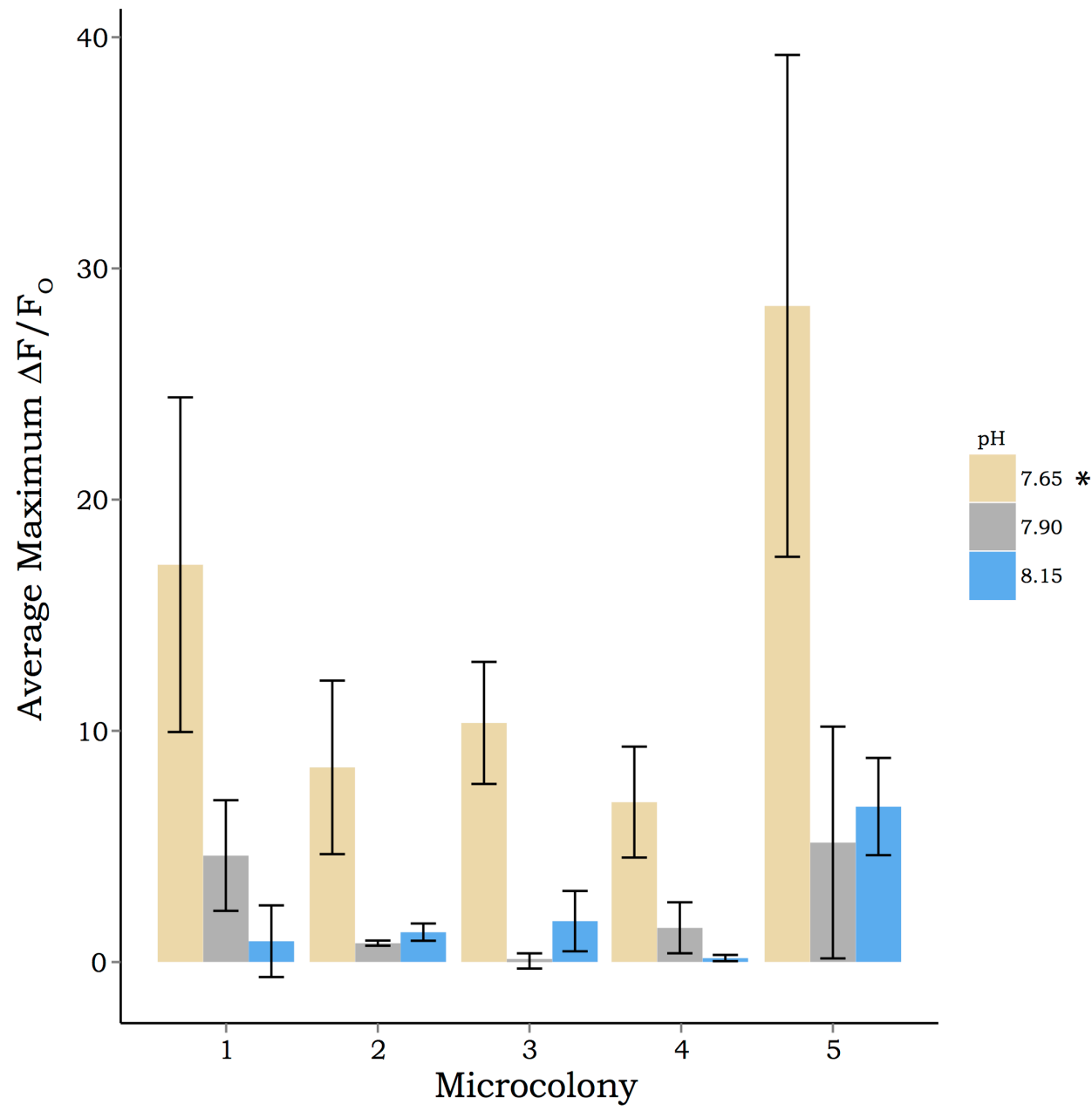


Figure 3.7 The average maximum normalized intensity value ($\Delta F/F_0$, F_0 being baseline fluorescence and ΔF being fluorescence change) for microcolonies of *Pavona maldivensis* at each pH. Microcolony numbers are arbitrary and were assigned prior to the experiment. A oneway ANOVA with blocking followed by a Tukey's post hoc test yielded a significant difference (p < 0.01) in the average maximum normalized intensity among pH treatments (8.15 versus 7.65, p = 0.004 and 7.90 versus 7.65, p = 0.004), but not among the microcolonies (p = 0.059). The results demonstrate that there is a ubiquitous treatment effect across microcolonies; all microcolonies responded to the pH changes in a similar manner. Asterisk (*) denotes statistical significance between the pH treatments. Error bars represent 95% bootstrapped confidence intervals: 10,000 bootstrapped samples/replicates reconstructed the mean normalized time series response curves across all the ROIs within each microcolony.

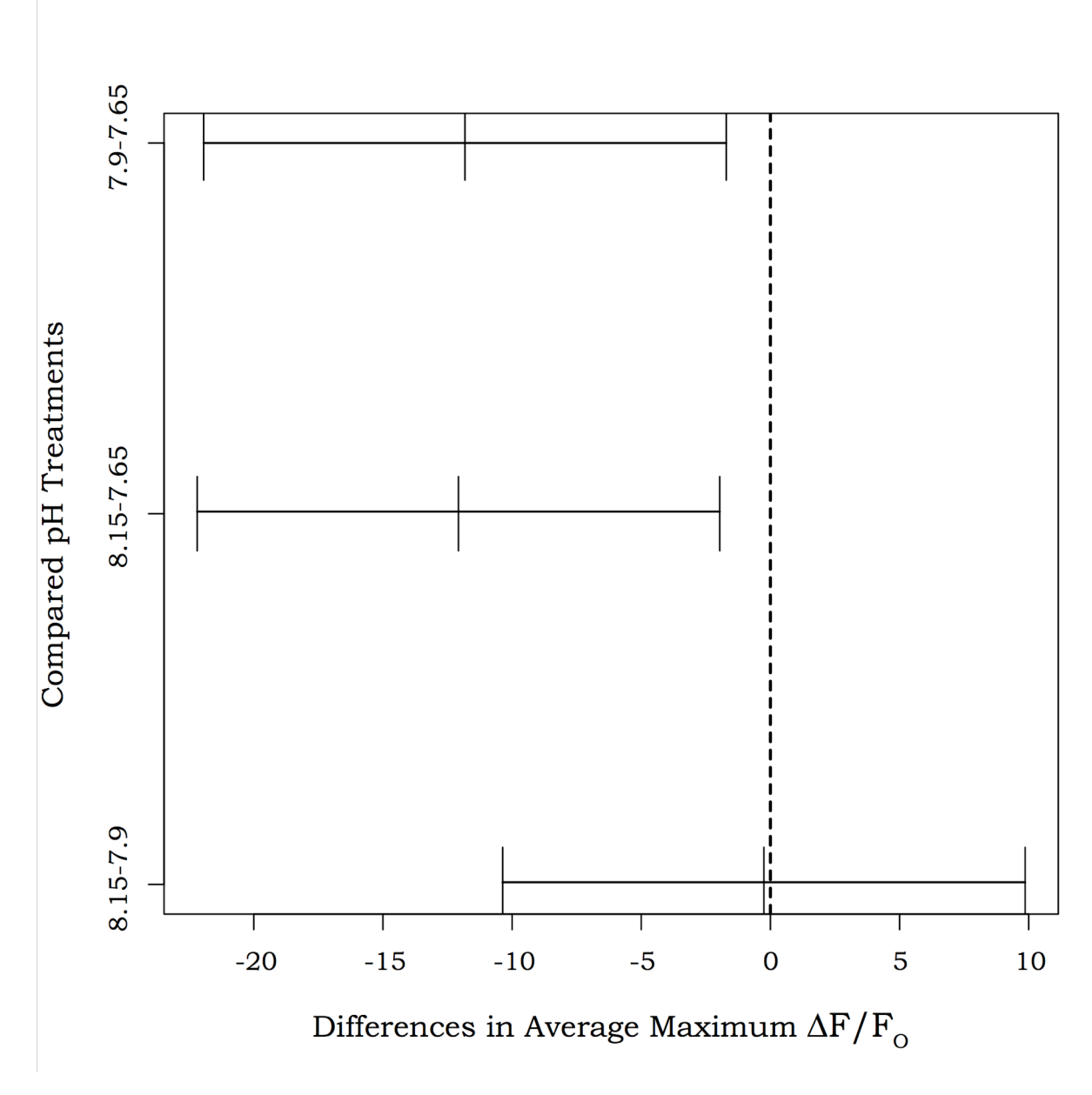


Figure 3.8 Tukey's 99% confidence intervals for *Pavona maldivensis*. This graphical representation of Tukey's post hoc test applied with a 99% confidence interval yields a pairwise difference between pH 8.15 and 7.65 (p = 0.004) and between pH 7.9 and 7.65 (p = 0.004). If the pairwise range contains zero, the difference between the pH treatments is not significant (p < 0.01).

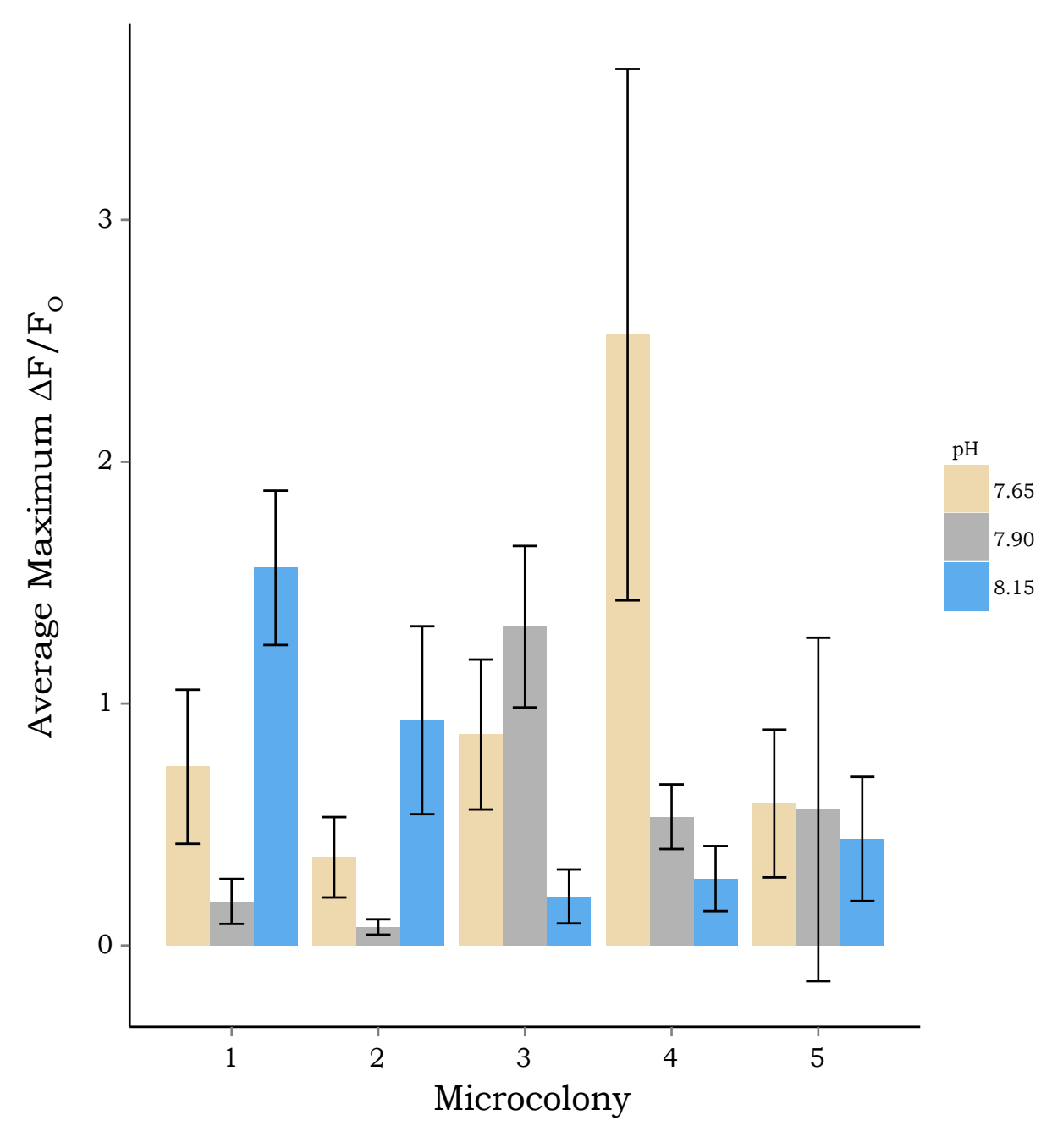


Figure 3.9 The average maximum normalized intensity value ($\Delta F/F_0$, F_0 being baseline fluorescence and ΔF being fluorescence change) for microcolonies of *Porites rus* at each pH. Microcolony numbers are arbitrary and were assigned prior to the experiment. A one-way ANOVA with blocking did not yield a significant difference (p < 0.05) in the average maximum normalized intensity among pH treatments (p = 0.593), or among microcolonies (p = 0.823). The results demonstrate that there is a ubiquitous lack of treatment effect across microcolonies; all microcolonies responded to the pH changes in a similar manner. Error bars represent 95% bootstrapped confidence intervals: 10,000 bootstrapped samples/replicates reconstructed the mean normalized time series response curves across all the ROIs within each microcolony.

Discussion

Calcium in the Calicodermis

The chief results of the current study demonstrate that ionomycin-activated calcium redistribution in the calicodermis responds differently to seawater acidification in *Pavona maldivensis* and *Porites rus*. *Pavona maldivensis* shows a significant difference among pH treatments, specifically between 8.15 and 7.65 (p = 0.004) and between 7.90 and 7.65 (p = 0.004). On the other hand, *Porites rus* does not show a significant difference (p = 0.593) among the pH treatments. By exposing coral microcolonies to Calcium Orange-AM, relative changes in the concentration of cytosolic calcium in response to ionomycin could be qualitatively mapped as a function of time. Changes in the qualitative mapping of the dynamic ionomycin-induced calcium response (dynamic calcium response) can be directly attributed to changes of pH for *Pavona maldivensis*, representative of present-to-future levels of ocean acidification.

As the two species studied are considered reef-building corals within a single Order of corals, one might expect microcolonies exposed to the exact same changes in pH would yield a similar dynamic calcium response. However, the pH dependence of the 50 µM ionomycin-induced calcium response curves differed between the two coral species, indicating that related species exhibit biological variation in response to the stimulus. The dynamic calcium response for *Porites rus* was consistent among all pH treatments, whereas the dynamic calcium response for *Pavona maldivensis* significantly differed among pH treatments.

The ionomycin-induced calcium response exhibited by *Pavona maldivensis* is phenomenologically similar to a calcium signaling response that is commonly found in vertebrates (Elzi et al. 2011; Verkhratsky and Parpura 2014). This well-studied phenomenon in vertebrate biology is known as store-operated calcium entry (SOCE) and is closely associated

with the endoplasmic reticulum (ER) and mitochondria-associated endoplasmic reticulum (MAM) calcium stores (Morgan and Jacob 1994; Huang and Putney 1998; Putney 2000; Kim et al. 2002, Herms et al. 2003; Hirohashi and Vacquier 2003; Parekh and Putney 2005; Parekh 2010; Rahman and Taylor 2010; Patergnani et al. 2011; Kaniewska et al. 2012; Suganuma et al. 2012; Shaw et al. 2013; Verhratsky and Parpura 2014). As reef-building corals contain abundant mitochondria in their calicodermal cells, it is plausible that *Pavona maldivensis* uses SOCE or a similar process for regulating intracellular calcium homeostasis, as the dynamic calcium response curves for *Pavona maldivensis* appear phenomenologically similar to those of vertebrate cells (Elzi et al. 2011; Verkhratsky and Parpura 2014).

The functional SOCE phenomenon that occurs across a multitude of ordinary vertebrate cells is represented by a biphasic calcium response (one example is illustrated by Figure 3.10): (1) an initial transient elevation of cytosolic calcium in response to the ionomycin stimulus and (2) a sustained plateau phase that gradually decays over time. In the calicodermis of *Pavona maldivensis* at a pH of 8.15, the same phenomenon of ionomycin inducing a biphasic calcium response is observed (Figure 3.11A). Upon observing the phenomenologically similar dynamic calcium responses for *Pavona maldivensis* (at pH 8.15) and vertebrate cells, I devised an *a posteriori* hypothesis.

I hypothesize that free cytosolic calcium may bear an intimate relationship with the MAM located in the calicodermal cells of *Pavona maldivensis* allowing for a process similar to the vertebrate SOCE. Induced calcium release via ionomycin or other stimuli induce downstream calcium signals associated with a process similar to SOCE. This process may play a vital role in regulating metamorphosis, calicodermal proliferation, symbiosis, and mineralization,

as calcium is a versatile second messenger (Bordat et al. 2004; DeSalvo et al. 2008; Grasso et al. 2008; Reyes-Bermudez et al. 2009; Grasso et al. 2011; Reyes-Bermudez et al. 2012).

As this is a proposed mechanism from an observational study, the detailed mechanism underlying SOCE may vary in terms of applying this phenomenon (as studied in vertebrates) to the calicodermal cells of reef-building coral, such as *Pavona maldivensis*. To potentially understand the phenomenon exhibited by *Pavona maldivensis*, one must begin to understand the underlying mechanisms involved with the SOCE phenomenon. The mechanisms of SOCE at the molecular level have only been recently mapped as a result of the research associated with vertebrate biology and physiology; therefore this proposed mechanism may vary in terms of applying the SOCE phenomenon to *Pavona maldivensis*.

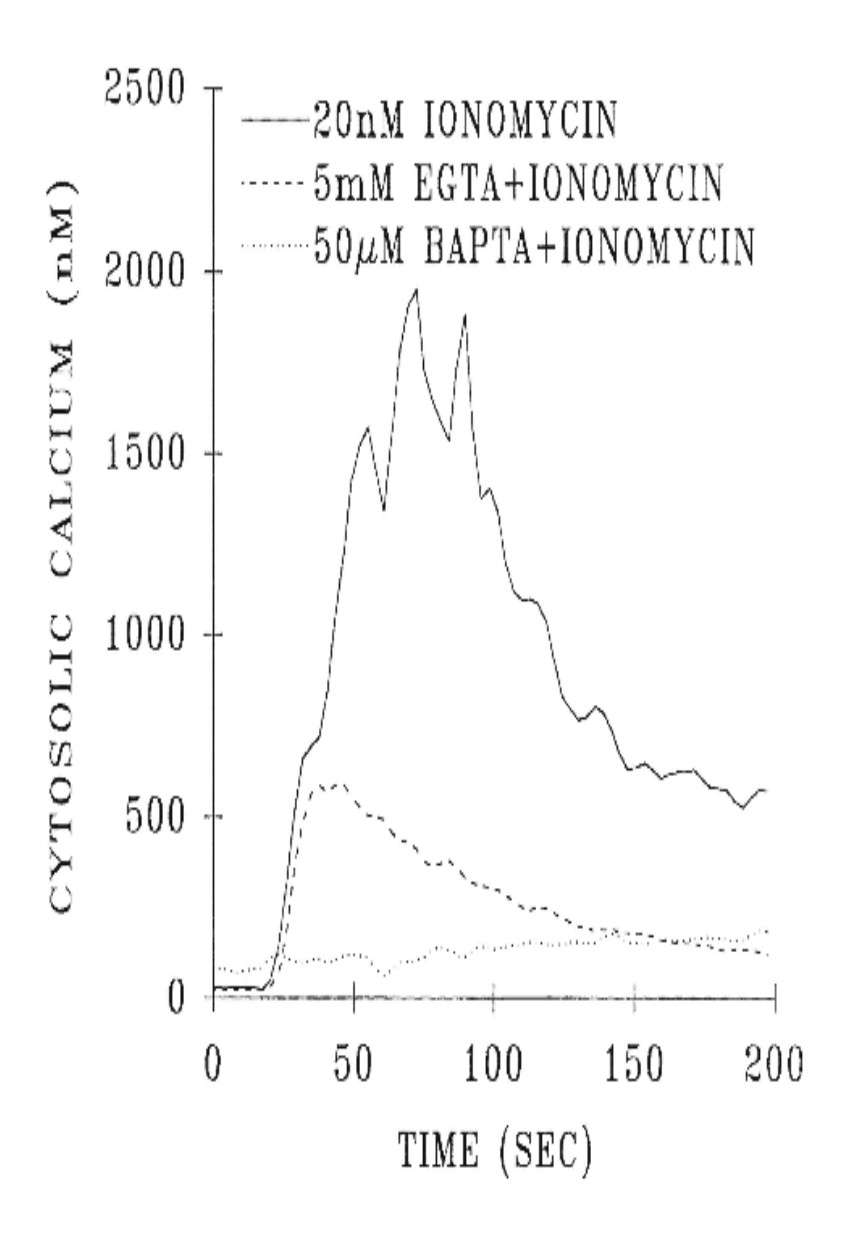


Figure 3.10 Ionomycin-induced calcium responses in vertebrate cells. The dynamic calcium response to ionomycin demonstrates a biphasic curve: (1) an initial transient elevation of cytosolic calcium in response to the ionomycin stimulus and (2) a sustained plateau phase that gradually tails off over time. This example illustrates one example of the functional expression of store-operated calcium entry (SOCE) in vertebrate cells. The above figure is from Elzi et al. (2001).

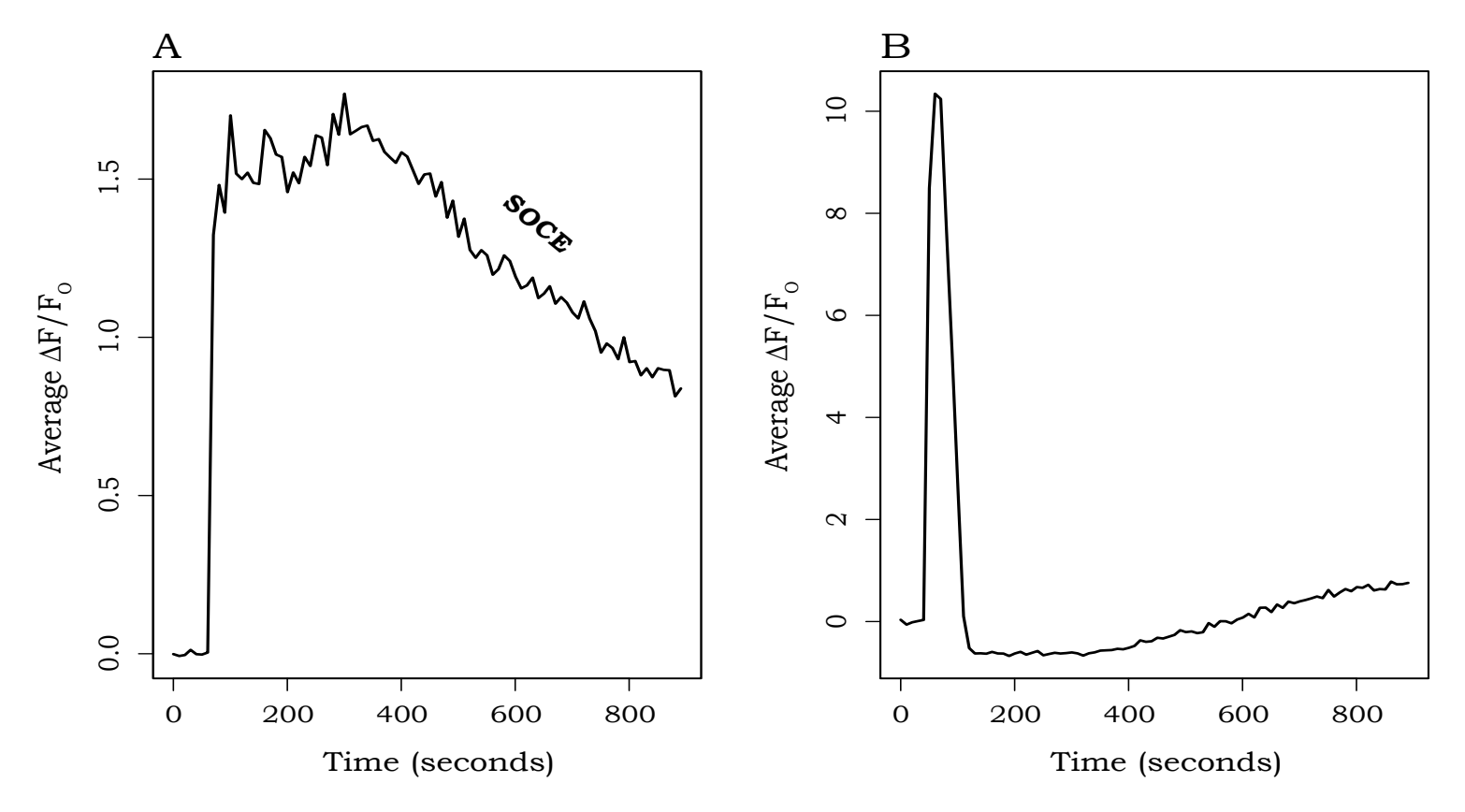


Figure 3.11 Average Normalized Calcium Response Curve for *Pavona maldivensis* microcolony 3: (A) The introduction of 50 μM ionomycin (at time = 40 seconds) into the environment of microcolony 3 at pH 8.15 results in a biphasic intracellular calcium response curve: (1) an initial transient elevation of cytosolic calcium within the calicodermis and (2) a sustained plateau phase that gradually decays over time. The plateau phase is entirely dependent upon extracellular calcium indicating the primary role of store-operated calcium entry (SOCE). Functional expression of SOCE represents the replenishing of MAM intracellular calcium stores upon depletion. (B) The introduction of 50μ M ionomycin into the environment of microcolony 3 (pH 7.65) results in a calcium response that is characteristic of cells in a calcium free extracellular medium: an initial transient elevation of cytosolic calcium within the calicodermis is not followed by the plateau phase. Thereby, exemplifying the effects of ocean acidification on calcium signaling responses within the calicodermis. Normalization was calculated against the baseline fluorescent intensity ($\Delta F/F_O$, F_O being baseline fluorescence and ΔF being fluorescence change) for all microcolonies.

Vertebrate Store-Operated Calcium Entry

Calcium signaling within and between cells contributes to a variety of biological functions: contractions of the heart, release of neurotransmitters, motility of the intestine, and activity of the immune system (Parekh 2010; Müller et al. 2013). To sustain calcium signaling throughout the life of a cell, gated calcium-permeable ion channels present in the plasma membrane play important roles for normal cellular function (Parekh 2010; Müller et al. 2013).

Simplistically, SOCE consists of the physiological mechanisms responsible for replenishing intracellular calcium stores upon depletion (Morgan and Jacob 1994; Huang and Putney 1998; Putney 2000; Kim et al. 2002, Herms et al. 2003; Hirohashi and Vacquier 2003; Parekh and Putney 2005; Parekh 2010; Rahman and Taylor 2010; Patergnani et al. 2011; Kaniewska et al. 2012; Suganuma et al. 2012; Shaw et al. 2013; Verhratsky and Parpura 2014). In nature, this occurs upon local stimulation of the G_q -protein plasma membrane receptor by a ligand protein (Parekh 2010; Patergnani et al. 2011; Kodama and Togari 2013). Activation of the G_q-protein induces downstream signaling that causes the ER and MAM calcium stores to be released into the cell's cytosol. The increased concentration of calcium, known as a calcium puff, inside the cell's cytosol evokes further downstream signaling. The initial release of ER and MAM calcium stores evokes a cascade effect, thereby releasing more of the ER and MAM calcium stores. This calcium puff may be used to initiate processes such as exocytosis, mitochondrial metabolism, gene expression, cell growth, proliferation and biomineralization (Parekh 2010; Cao et al. 2013). Because the ER and MAM calcium stores deplete, mechanisms are needed to replenish these stores.

When the calcium puff increases cytosolic calcium, two mechanisms work synergistically to restore calcium homeostasis within the cell (cytosol and calcium store). The plasma

membrane associated calcium ATP-ase (PMCA) moves calcium from the cytosol to the extracellular medium. Simultaneously, some of the cytosolic calcium is returned to the ER and MAM calcium stores by the sarco/endoplasmic reticulum calcium ATPase (SERCA). However, not all the released calcium will be re-bound by the ER or MAM calcium stores, meaning if the above processes were to be repeated over and over without replenishment of cytosolic calcium, then the ER and MAM calcium stores would eventually deplete and calcium signaling would stop (Huang and Putney 1998; Zoccola et al. 2004; Parekh and Putney 2005; Rahman and Taylor 2010; Patergnani et al. 2011; Cao et al. 2013; Verhratsky and Parpura 2014).

Depletion of ER and MAM calcium stores is avoided by the communication of the stromal interaction molecule 1 (STIM1), located in the ER and MAM membranes, and ORAI proteins in the cell's plasma membrane (Parekh and Putney 2005; Smyth et al. 2011; Saganuma et al. 2012; Feske 2013; Müller et al. 2013; Shaw et al. 2013; Verkhratsky and Parpura 2014). The communication of these proteins induces a permeable calcium channel (ORAI channel) to open in the plasma membrane. Calcium moves through the ORAI channel as the concentration and electrochemical gradient highly favors calcium movement from the extracellular medium to the cell's cytosol (Morgan and Jacob 1994; Huang and Putney 1998; Hirohashi and Vacquier 2003; Parekh and Putney 2005; Rahman and Taylor 2010; Patergnani et al. 2011; Kaniewska et al. 2012; Suganuma et al. 2012; Cao et al. 2013; Feske 2013; Shaw et al. 2013; Verhratsky and Parpura 2014). As calcium enters the cell's cytosol via the ORAI channel, the concentration of cytosolic calcium remains high until the SERCA pumps begin to move calcium from the cytosol back into the ER and MAM calcium stores. The entire SOCE process restores the ER and MAM calcium stores to their original resting state.

Biphasic SOCE Response in Pavona maldivensis

The dynamic ionomycin-induced calcium response for *Pavona maldivensis* illustrates the SOCE phenomenon. When ionomycin is introduced, the MAM intracellular calcium stores release calcium into the calicodermal cytosol. This is recognizable as the transient upward spike in fluorescent intensity (Figure 3.11A). Extracellular calcium is then added to the calicodermal cytosol via the opening of proteins in the plasma membrane. This helps maintain a relatively stable concentration of calcium within the cytosol, recognizable as the sustained plateau in fluorescent intensity (Figure 3.11A). The SERCA pump then moves calcium from the calicodermal cytosol into the ER and MAM calcium stores, recognizable as the gradual decline in fluorescent intensity after the plateau phase (Figure 3.11A). The gradual decline in the concentration of cytosolic calcium continues until the ER and MAM calcium stores are restored to their original state; therefore representing the functional expression of the SOCE phenomenon.

In comparison, Figure 3.11B, microcolony 3 at a pH of 7.65, demonstrates the initial transient response to 50μM ionomycin (Figure 3.11B), but does not illustrate a sustained plateau phase. Figure 3.11B closely resembles the ionomycin-induced calcium response curve from cells imaged in a calcium free extracellular medium (Cornell-Bell et al. 1990; Parekh and Putney 2005; Suganuma et al. 2012; Müller et al. 2013; Verhratsky and Parpua 2014). As these trials were not conducted in a calcium free extracellular medium, Figure 3.11B suggests that the transport of calcium into the calicodermal cytoplasm via the associated plasma membrane proteins was suppressed due to the slow rise in the average normalized fluorescent intensity back towards the fluorescent baseline. This phenomenon raises a major concern for calcium signaling within the coral during times of increased ocean acidification. When the corals are stimulated to release intracellular stores, the functional SOCE phenomenon may be suppressed or even

inhibited by the more acidic environments associated with ocean acidification as represented by Figure 3.11B. If this process were to continue, then the ER and MAM calcium would eventually deplete and calcium signaling would stop. This would lead to many cellular abnormalities and eventually necrosis (Parekh and Putney 2005; Pimentel et al. 2012; Logan et al. 2014).

Conclusion

As climate change progresses, it is highly probable that many of the inhabitants of the tropical reef ecosystems will be pushed beyond their lethal limits within the next century (Hoegh-Guldberg et al. 2007; Tewksbury et al. 2008; Putron et al. 2010; IPCC 2014). Calcium signaling and homeostasis are major concerns for reef-building coral as anthropogenic CO₂ emissions increase and the pH of the oceans becomes more acidic with a lower [CO₃²⁻] (Hoegh-Guldberg 2007; Feely et al. 2009; Hönisch et al. 2012; Kaniewska et al. 2012; Roleda et al. 2012). The results of this study indicate that ocean acidification affects calcium signaling within the calicodermis of *Pavona maldivensis*. Additionally, the ionomycin-induced calcium response curves among the different pH treatments for Pavona maldivensis appeared to be phenomenologically similar to the vertebrate calcium signaling mechanism, SOCE. In the most acidic environment I tests, pH 7.65, it appears the calcium signaling of the calicodermis was suppressed and/or inhibited. This may imply that reef-building coral using a similar mechanism (SOCE) to regulate intracellular calcium in the calicodermis may not have exhibit proper cellular functions, one example being biomineralization, in an acidified environment. To better understand and fully evaluate the SOCE phenomenon that was demonstrated by Pavona maldivensis in relation to present-future ocean acidification, further molecular studies should be implemented. Additionally, this study demonstrated the biological variation between Pavona maldivensis and Porites rus. This variation has important implications for studying the effects of ocean acidification, as these species may not necessarily reflect a generalized conclusion for all reef-building coral.

REFERENCES

REFERENCES

- Ainsworth TD, Hoegh-Guldberg O. 2008. Cellular processes of bleaching in the Mediterranean coral *Oculina patagonica*. Coral Reefs 27: 593–597.
- Allemand D, Ferrier-Pagès C, Furla P, Houlbrèque F, Puverel S, Reynaud S, Tambutté E, Tambutté S, Zoccola D. 2004. Biomineralisation in reef-building corals: from molecular mechanisms to environmental control. Comptes. Rendus. Palevol. 3: 453–467.
- Allemand D, Tambutté É, Zoccola D, Tambutté S. 2011. Coral Reefs: An Ecosystem in Transition. Dordrecht: Springer Netherlands.
- Anthony KRN, Kline DI, Diaz-Pulido G, Dove S, Hoegh-Guldberg O. 2008. Ocean acidification causes bleaching and productivity loss in coral reef builders. Proceedings of the National Academy of Sciences of the United States of America 105: 17442–17446.
- Antonius A. 1985. Coral disease in the Indo-Pacific: a first record. Marine Ecology 6(3): 197-218.
- Balmaseda M a., Trenberth KE, Källén E. 2013. Distinctive climate signals in reanalysis of global ocean heat content. Geophysical Research Letters 40: 1754–1759.
- Barnes DJ. 1970. Coral skeletons: An explanation of their growth and structure. Science 170: 1305–1308.
- Barnes DJ. 1972. The structure and formation of growth-ridges in scleractinian coral skeletons. Proc. R. Soc. London, Ser. B 182: 331–350.
- Barnes DJ. 1985. The effect of photosynthetic and respiratory inhibitors upon calcification in the staghorn coral, *Acropora formosa*. In: Delesalle B, Galzin R, Salvat B (eds) Proceeding of the fifth international coral reef congress. Museum National d'Histoire Naturelle (National Museum of Natural History) and the Ecole Pratique des Hautes Etudes (Practical School of Advanced Studies), Tahiti, 161–166.
- Barber J. 2007. Biological solar energy. Philosophical transactions. Series A, Mathematical, physical, and engineering sciences 365: 1007–1023.
- Bellwood DR, Goatley CHR, Brandl SJ, Bellwood O. 2014. Fifty million years of herbivory on coral reefs: fossils, fish and functional innovations. Proc. R. Soc. B 281: 20133046.
- Berridge MJ, Loschman J. 1972. Transporting epithelia. Academic, New York.
- Bindoff NL, Willebrand J, Artale VAC, Gregory J, Gulev S, Hanawa K, Quéré CL, Levitus S, Nojiri Y, Shum CK, Talley LD, Unnikrishnan A. 2007. Observations: oceanic climate change and sea level. In: Climate change 2007: the physical science basis. Contribution of

- Working Group I to the Fourth Assessment Report of the Intergovernmental Panel on Climate Change. Cambridge University Press, Cambridge.
- Bordat C, Guerquin-Kern JL, Lieberherr M, Gournot G. 2004. Direct visualization of intracellular calcium in rat osteoblasts by energy-filtering transmission electron microscopy. Histochem. Cell Biol. 121: 131- 138.
- Bouillon J, Coppois G. 1977. Etude comparative de la mésoglée des Cnidaires. Cah. Biol. Mar. XVIII 3: 339–368.
- Bousquet P, Peylin P, Ciais P, Le Queré C, Friedlingstein P. 2000. Regional changes in carbon dioxide fluxes of land and oceans since 1980. Science 290: 1342-1346.
- Brini M, Carafoli E. 2000. Calcium signaling: a historical account, recent developments and future perspectives. Cell. Mol. Life Sci. 57: 354- 370.
- Broadgate W. 2012. Ocean acidification summary for policymakers: Third Symposium on the Ocean in a high CO2 world.
- Budd AF, Romano SL, Smith ND, Barbeitos MS. 2010. Rethinking the phylogeny of scleractinian corals: a review of morphological and molecular data. Integrative and comparative biology 50: 411–27.
- Caldeira K, Wickett ME. 2003. Anthropogenic carbon and ocean pH. Nature 425: 365.
- Caldeira K. 2005. Ocean model predictions of chemistry changes from carbon dioxide emissions to the atmosphere and ocean. Journal of Geophysical Research 110: C09S04.
- Caldeira K, Archer D, Barry JP, Bellerby RGJ, Brewer PG, Cao L, Dickson AG, Doney SC, Elderfield H, Fabry VJ, Feely R a., Gattuso J-P, Haugan PM, Hoegh-Guldberg O, Jain AK, Kleypas J a., Langdon C, Orr JC, Ridgwell A, Sabine CL, Seibel B a., Shirayama Y, Turley C, Watson AJ, Zeebe RE. 2007. Comment on "Modern-age buildup of CO₂ and its effects on seawater acidity and salinity" by Hugo A. Loáiciga. Geophysical Research Letters 34: L18608.
- Chalker BE. 1976. Calcium transport during skeletogenesis in hermatypic corals. Comp. Biochem. Physiol. 54A: 455–459.
- Chalker BE, Taylor DL. 1975. Light-enhanced calcification, and the role of oxidative phosphorylation in calcification of the coral *Acropora cervicornis*. Proc. R. Soc. Lond. B 190: 323–331.
- Chevrier R, Meyssignac B, Bourgeois E, Marzeion B, Cazenave A. 2014. Regional Variability of the 20th century sea level rise from Ocean-Atmosphere Coupled Climate Models. Geological Research 16: 7540

- Church JA, White NJ, Konikow LF, Domingues CM, Cogley JG, Rignot E, Gregory JM, van den Broeke MR, Monaghan AJ, Velicogna I. 2011. Revisiting the earth's sea-level and energy budgets from 1961 to 2008. Geophysical Research Letters 38: L18601.
- Cohen AL, McConnaughey TA. 2003. Geochemical perspectives on coral mineralization. Rev. Mineral Geochem. 54:151–187.
- Connie Lam CMC, Yeung PKK, Wong JTY. 2005. Monitoring cytosolic calcium in the dinoflagellate *Crypthecodinium cohnii* with calcium orange-AM. Plant Cell Physiol. 46(6):1021-1027.
- Cornell-Bell AH, Finkbeiner SM, Cooper MS, Smith SJ. 1990. Glutamate induces calcium waves in cultured astrocytes: long-range glial signaling. Science 247: 470–473.
- Courchamp F, Hoffmann BD, Russell JC, Leclerc C, Bellard C. 2014. Climate change, sea-level rise, and conservation: keeping island biodiversity afloat. Trends in Ecology & Evolution 29: 127–130.
- Crossland CJ, Hatcher BG, Smith SV. 1991. Role of coral reefs in global ocean production. Coral Reefs 10: 55-64.
- Davis WM. 1928. The coral reef problem. Am. Geogr. Soc. 9: 1-596.
- De Putron SJ, McCorkle DC, Cohen AL, Dillon AB. 2010. The impact of seawater saturation state and bicarbonate ion concentration on calcification by new recruits of two Atlantic corals. Coral Reefs 30: 321–328.
- Dedkova EN, Sigova AA, Zinchenko VP. 2000. Mechanism of action of calcium ionophores on intact cells: ionophore-resistant cells. Membr. Cell. Biol. 13(3): 357–368.
- DeSalvo MK, Sunagawa S, Fisher PL, Voolstra CR, Iglesias-Prieto R, Medina M. 2010. Coral host transcriptomic states are correlated with *Symbiodinium* genotypes. Molecular Ecology 19: 1174–1186.
- Domingues CM, Church JA, White NJ, Gleckler PJ, Wijffels SE, Barker PM, Dunn JR. 2008. Improved estimates of upper-ocean warming and multi-decadal sea-level rise. Nature 453: 1090–1093.
- Doney SC, Fabry VJ, Feely RA, Kleypas JA. 2009. Ocean acidification: the other CO₂ problem. Ann. Rev. Mar. Sci. 1: 169–192.
- Donner SD, Potere D. 2007. The Inequity of the Global Threat to Coral Reefs. BioScience 57: 214-215.
- Dunn KW, Kamocka MM, McDonald JH. 2011. A practical guide to evaluating colocalization in biological microscopy. Am. J. Physiol. Cell Physiol. 300(4): C723-742.

- Edmunds P. 2010. Population biology of *Porites astreoides* and *Diploria strigosa* on a shallow Caribbean reef. Mar. Ecol. Prog. Ser. 418: 87–104.
- Edmunds PJ. 2011. Zooplanktivory ameliorates the effects of ocean acidification on the reef coral *Porites spp*. Limnology and Oceanography 56: 2402–2410.
- Erez J, Braun A. 2007. Calcification in hermatypic corals is based on direct seawater supply to the biomineralization site. In: Goldschmidt Conference Abstracts 2007 Cologne, Germany, A260.
- Fabricius KE. 2011. Losers and winners in coral reefs acclimatized to elevated carbon dioxide concentrations. Nature Clim. Change 1: 165–169.
- Fautin DG, Mariscal RN. 1991. Cnidaria: Anthozoa. In: Harrison, F.W., Westfall, J.A. (Eds.), Placozoa, Porifera, Cnidaria, and Ctenophora. Wiley-Liss, New York, 267–358.
- Feely RA, Doney SC, Cooley SR. 2009. Ocean acidification: present conditions and future changes in a high-CO2 world. Oceanography 22 (4): 36e47.
- Fröhlich C. 1991 History of solar radiometry and the world radiometric reference. Metrologia 28: 111-115.
- Furla P, Allemand D, Orsenigo MN. 2000a. Involvement of H⁺-ATPase and carbonic anhydrase in inorganic carbon uptake for endosymbiont photosynthesis. Am. J. Physiol. (Regul. Integr. Comp.) 278: R870–R881.
- Furla P, Galgani I, Durand I, Allemand D. 2000b. Sources and mechanisms of inorganic carbon transport for coral calcification and photosynthesis. The Journal of Experimental Biology 203: 3445–3457.
- Galloway SB, Work TM, Bochsler VS, Harley RA, Kramarsky-Winters E, McLaughlin SM, Meteyer CU, Morado JF, Nicholson JH, Parnell PG, Peters EC, Reynolds TL, Rotstein DS, Sileo L, Woodley CM. 2006. A Report of the CDHC Coral Histopathology Workshop II. National Oceanic and Atmospheric Administration, Silver Spring, 88.
- Glynn PW. 1976. Some physical and biological determinants of coral community structure in the eastern Pacific. Ecol. Monogr. 46: 431-456.
- Glynn PW, D'Croz L. 1990. Experimental evidence for high temperature stress as the cause of El Niño-coincident coral mortality. Coral Reefs 8: 181-191.
- Goatley CHR, Bellwood DR, Bellwood O. 2010 Fishes on coral reefs: changing roles over the past 240 million years. Paleobiology 36: 415–427.
- Goldberg W.M. 2001. Acid polysaccharides in the skeletal matrix and calicoblastic epithelium of the stony coral *Mycetophyllia reesi*. Tissue Cell 33(4): 376–387.

- Grasso LC, Maindonald J, Rudd S, Hayward DC, Saint R, Miller DJ, Ball EE. 2008. Microarray analysis identifies candidate genes for key roles in coral development. BMC Genomics 9: 540.
- Grasso LC, Negri AP, Foret S, Saint R, Hayward DC, Miller DJ, Ball EE. 2011. The biology of coral metamorphosis: molecular responses of larvae to inducers of settlement and metamorphosis. Dev. Biol. 353(2): 411–419.
- Guemas V, Doblas-Reyes FJ, Andreu-Burillo I, Asif M. 2013. Retrospective prediction of the global warming slowdown in the past decade. Nat. Clim. Chang. 3(7): 649-653.
- Gusakova MA, Karlin LN. 2014. Assessment of contribution of greenhouse gases, water vapor, and cloudiness to the variations of global surface air temperature. Russ. Meteorol. Hydrol. 39(3): 146-151.
- Hayes RL, Goreau NI. 1977. Intracellular crystal-bearing vesicles in the epidermis of scleractinian corals, *Astrangia danae* (Agassiz) and *Porites porites* (Pallas). Biol. Bull. 152: 26–40.
- Hayes RL, Bush PG. 1990. Microscopic observations of recovery in the reef-building scleractinian coral, *Montipora annularis*, after bleaching on Cayman reef. Coral Reefs 8: 203-209.
- Heidelberg KB, Sebens KP, Purcell JE. 2004. Composition and sources of near reef zooplankton on a Jamaican forereef along with implications for coral feeding. Coral Reefs 23(2): 263-276.
- Hoegh-Guldberg O. 1999. Climate change, coral bleaching and the future of the world's coral reefs. Marine and Freshwater Research 50: 839–866.
- Hoegh-Guldberg O. 2010. Coral reef ecosystems and anthropogenic climate change. Regional Environmental Change 11: 215–227.
- Hoegh-Guldberg O, Mumby PJ, Hooten AJ, Steneck RS, Greenfield P, Gomez E, Harvell CD, Sale PF, Edwards AJ, Caldeira K, Knowlton N, Eakin CM, Iglesias-Prieto R, Muthiga N, Bradbury RH, Dubi A, Hatziolos ME. 2007. Coral reefs under rapid climate change and ocean acidification. Science 318: 1737–1742.
- Hoenderop JG, Nilius B, Bindels RJ. 2005. Calcium absorption across epithelia. Physiol. Rev. 85: 373-422.
- Hönisch B, Ridgwell A, Schmidt DN, Thomas E, Gibbs SJ, Sluijs A, Zeebe R, Kump L, Martindale RC, Greene SE, Kiessling W, Ries J, Zachos JC, Royer DL, Barker S, Marchitto TM, Moyer R, Pelejero C, Ziveri P, Foster GL, Williams B. 2012. The geological record of ocean acidification. Science 335: 1058–1063.

- Houghton RA. 2007. Balancing the global carbon budget. Annual Review of Earth and Planetary Science 35: 313–347.
- Huang Y, Putney JW. 1998. Relationship between Intracellular calcium store depletion and calcium release-activated calcium current in a mast cell line (RBL-1). Journal of Biological Chemistry 273: 19554–19559.
- IPCC. 2014. Climate Change 2014: Impacts, Adaptation, and Vulnerability. Part A: Global and Sectoral Aspects. Contribution of Working Group II to the Fifth Assessment Report of the Intergovernmental Panel on Climate Change [Field, C.B., V.R. Barros, D.J. Dokken, K.J. Mach, M.D. Mastrandrea, T.E. Bilir, M. Chatterjee, K.L. Ebi, Y.O. Estrada, R.C. Genova, B. Girma, E.S. Kissel, A.N. Levy, S. MacCracken, P.R. Mastrandrea, and L.L. White (eds.)]. Cambridge University Press, Cambridge, United Kingdom and New York, NY, USA, 1132 pp.
- Jackson JBC. 1991. Diversity of in resource use and life patterns result from species differences histories and from disturbances. Bioscience 41: 475–482.
- Johnston IS. 1980. The ultrastructure of skeletogenesis in hermatypic corals. Int. Rev. Cytol. 67: 171-214.
- Jokiel PL, SL Coles. 1990. Response of Hawaiian and other Indo-Pacific reef corals to elevated temperature. Coral Reefs 8:155-162.
- Jones RJ, Hoegh-Guldberg O. 2001. Diurnal changes in the photochemical efficiency of the symbiotic dinoflagellates (Dinophyceae) of corals: photoprotection, photoinactivation and the relationship to coral bleaching. Plant, Cell & Environment 24(1): 89–99.
- Kaniewska P, Campbell PR, Kline DI, Rodriguez-Lanetty M, Miller DJ, Dove S, Hoegh-Guldberg O. 2012. Major cellular and physiological impacts of ocean acidification on a reef building coral. PloS ONE 7(4): e34659.
- Karoonuthaisiri N, Titiyevskiy K, Thomas JL. 2003. Destabilization of fatty acid-containing liposomes by polyamidoamine dendrimers. Colloids. Surf. B 27:365–375.
- Keeling CD, Piper SC, Bacastow RB, Wahlen M, Whorf TP, Heimann M, Meijer HA. 2005. Exchanges of atmospheric CO2 and 13CO2 with the terrestrial biosphere and oceans from 1978 to 2000. A History of Atmospheric CO₂ and its Effects on Plants, Animals, and Ecosystems Ecological Studies 177: 83-113.
- Keeling CD, Whorf TP, Wahlen M, Van der Pilchtt J. 1995. Interannual extremes in the rate of rise of atmospheric carbon dioxide since 1980. Nature 375: 666–670.
- Khatiwala S, Tanhua T, Fletcher SM, Gerber M, Doney SC, Graven HD, Gruber N, McKinley GA, Murata A, Ríos AF, Sabine CL. 2013. Global ocean storage of anthropogenic carbon. Biogeosciences 10: 2169–2191.

- Kottra G, Frömter E. 1983. Functional properties of the paracellular pathway in some leaky epithelia. The Journal of Experimental Biology 106: 217–229.
- Kroeker K, Kordas R, Crim R. 2010. Meta-analysis reveals negative yet variable effects of ocean acidification on marine organisms. Ecology Letters 13: 1419–1434.
- Le Quesne WJF, Pinnegar JK. 2011. The potential impacts of ocean acidification: scaling from physiology to fisheries. Fish and Fisheries 13: 333–344.
- Lesser MP. 1996. Elevated temperatures and ultraviolet radiation cause oxidative stress and inhibit photosynthesis on symbiotic dinoflagellates. Limnology and Oceanography 41(2): 271-283.
- Logan CV, Szabadkai G, Sharpe JA, Parry DA, Torelli S, Childs AM, Kriek M, Phadke R, Johnson CA, Roberts NY, Bonthron DT, Pysden KA, Whyte T, Munteanu I, Foley AR, Wheway G, Szymanska K, Natarajan S, Abdelhamed Z a, Morgan JE, Roper H, Santen GWE, Niks EH, van der Pol WL, Lindhout D, Raffaello A, De Stefani D, den Dunnen JT, Sun Y, Ginjaar I, Sewry CA, Hurles M, Rizzuto R, Duchen MR, Muntoni F, Sheridan E. 2014. Loss-of-function mutations in MICU1 cause a brain and muscle disorder linked to primary alterations in mitochondrial calcium signaling. Nature Genetics 46: 188–193.
- Lough JM. 2008. 10th Anniversary Review: a changing climate for coral reefs. J. Environ. Monit. 10(1):21-29.
- Loya Y, Sakai K, Yamazato K, Nakano Y, Sambali H, Van Woesik R. 2001. Coral bleaching: The winners and the losers. Ecology Letters 4: 122–131.
- Lüthi D, Le Floch M, Bereiter B, Blunier T, Barnola J-M, Siegenthaler U, Raynaud D, Jouzel J, Fischer H, Kawamura K, Stocker TF. 2008. High-resolution carbon dioxide concentration record 650,000-800,000 years before present. Nature 453:379–382.
- Marshall AT, Wright OP. 1993. Confocal laser scanning light microscopy of the extra-thecal epithelia of undecalcified scleractinian corals. Cell & Tissue Research 272: 533–543.
- Marshall AT. 1996. Calcification in hermatypic and ahermatypic corals. Science 271:637–639.
- Marshall AT, Clode PL, Russell R, Prince K, Stern R. 2007. Electron and ion microprobe analysis of calcium distribution and transport in coral tissues. The Journal of Experimental Biology 210: 2453–63.
- Marubini F, Ferrier-Pagès C, Furla P, Allemand D. 2008. Coral calcification responds to seawater acidification: a working hypothesis towards a physiological mechanism. Coral Reefs 27: 491–499.
- Moberg F, Folke C. 1999. Ecological goods and services of coral reef ecosystems. Ecological Economics 29: 215–233.

- Morgan AJ, Jacob R. 1994. Ionomycin enhances Ca2+ influx by stimulating store-regulated cation entry and not by a direct action at the plasma membrane. The Biochemical Journal 300(3): 665–672.
- Müller MS, Obel LF, Waagepetersen HS, Schousboe A, Bak LK. 2013. Complex actions of ionomycin in cultured cerebellar astrocytes affecting both calcium-induced calcium release and store-operated calcium entry. Neurochemical Research 38: 1260–1265.
- Munday PL, Dixson DL, Donelson JM, Jones GP, Pratchett MS, Devitsina G V, Døving KB. 2009. Ocean acidification impairs olfactory discrimination and homing ability of a marine fish. Proceedings of the National Academy of Sciences of the United States of America 106: 1848–1852.
- Murray J, Irvine R. 1891. Coral reefs and other carbonate of lime formations in modern seas. Proceedings of the Royal Society of Edinburgh 79–109.
- Muscatine L. 1990. The role of symbiotic algae in carbon and energy flux in reef corals. In Coral reefs, ecosystems of the world (ed. Z. Dubinsky) 75–87. Amsterdam: Elsevier Science.
- Muscatine L, Tambutté E, Allemand D. 1997. Morphology of coral desmocytes, cells that anchor the calicoblastic epithelium to the skeleton. Coral Reefs 16: 205–213.
- Ohmura A, Gilgen H, Hegner H, Müller G, Wild M, Dutton EG, Forgan B, Fröhlich C, Philipona R, Heimo A, König-Langlo G, McArthur B, Pinker R, Whitlock CH, Dehne K. 1998. Baseline Surface Radiation Network (BSRN/WCRP): New precision radiometry for climate research. Bulletin of the American Meteorological Society 79: 2115–2136.
- Pandolfi JM, Connolly SR, Marshall DJ, Cohen AL. 2011. Projecting coral reef futures under global warming and ocean acidification. Science 333: 418–422.
- Parekh AB, Putney JW. 2005. Store-operated calcium channels. Physiological reviews 85: 757–810.
- Pecorino D, Barker MF, Dworjanyn S a., Byrne M, Lamare MD. 2013. Impacts of near future sea surface pH and temperature conditions on fertilisation and embryonic development in Centrostephanus rodgersii from northern New Zealand and northern New South Wales, Australia. Marine Biology 161: 101–110.
- Philipona R. 2013. Atmospheric thermal radiation from historical measurements to investigations of the Earth's greenhouse effect. Meteorologische Zeitschrift 22: 771–775.
- Philipona R, Dutton EG, Stoffel T, Michalsky J, Reda I, Stifter A, Wendling P, Wood N, Clough SA, Mlawer EJ, Anderson G, Revercomb HE, Shippert TR. 2001. Atmospheric longwave irradiance uncertainty: Pyrgeometers compared to an absolute sky-scanning radiometer, atmospheric emitted radiance interferometer, and radiative transfer model calculations. Journal of Geophysical Research 106: 129–142.

- Philipona R, Kräuchi A, Brocard E. 2012. Solar and thermal radiation profiles and radiative forcing measured through the atmosphere. Geophysical Research Letters 39: L13806.
- Ramanathan V, Cess RD, Harrison EF, Minnis P, Barkstorm BR, Ahmad E, Hartmann D. 1989. Cloud-radiative forcing and climate: results from the earth radiation budget experiment. Science 243: 57-63.
- Raval A, Ramanathan V. 1989. Observational determination of the greenhouse effect. Nature 342: 758–761.
- Reyes-Bermudez A, Miller DJ, Sprungala S. 2012. The neuronal calcium sensor protein acrocalcin: a potential target of calmodulin regulation during development in the coral *Acropora millepora*. PloS ONE 7: e51689.
- Roleda MY, Boyd PW, Hurd CL. 2012. Before Ocean Acidification: Calcifier Chemistry Lessons 1. Journal of Phycology 48: 840–843.
- Schmid V, Ono S, Reber-Muller S. 1999. Cell-substrate interactions in cnidaria. Microsc. Res. Tech. 44: 254–268.
- Shinzato C, Shoguchi E, Kawashima T, Hamada M, Hisata K, Tanaka M, Fujie M, Fujiwara M, Koyanagi R, Ikuta T, Fujiyama A, Miller DJ, Satoh N. 2011. Using the *Acropora digitifera* genome to understand coral responses to environmental change. Nature 476: 320–323.
- Slusarski DC, Pelegri F. 2007. Calcium signaling in vertebrate embryonic patterning and morphogenesis. Developmental Biology 307: 1–13.
- Solomon S, Qin D, Manning M, Chen Z, Marquis M, Averyt KB, Tignor M, Miller HL. 2007. Climate Change 2007: The Physical Science Basis. Cambridge University Press, Cambridge, UK.
- Spalding MD, Ravilious C, Green EP. 2001. World atlas of coral reefs. Prepared by the UNEP World Conservation Monitoring Centre. University Press of California Press: Berkeley, USA.
- Spalding MD, Grenfell AM. 1997. New estimates of global and regional coral reef areas. Coral Reefs 16: 225–230.
- Suganuma N, Ito S, Aso H, Kondo M, Sato M, Sokabe M, Hasegawa Y. 2012. STIM1 regulates platelet-derived growth factor-induced migration and Ca2+ influx in human airway smooth muscle cells. PloS ONE 7: e45056.
- Sundquist ET. 1993. The global carbon dioxide budget. Science 259: 934–941.
- Takahashi A, Camacho P, Lechleiter JD, Herman B. 1999. Measurement of intracellular calcium. Physiological Reviews 79: 1089–1125.

- Tambutté É, Allemand D, Bourge I, Gattuso JP, Jaubert J. 1995. An improved 45 Ca protocol for investigating physiological mechanisms in coral calcification. Marine Biology 122: 453–459.
- Tambutté E, Tambutté S, Segonds N, Zoccola D, Venn A, Erez J, Allemand D. 2012. Calcein labelling and electrophysiology: insights on coral tissue permeability and calcification. Proceedings. Biological Sciences / The Royal Society 279: 19–27.
- Tambutté S, Holcomb M, Ferrier-Pagès C, Reynaud S, Tambutté É, Zoccola D, Allemand D. 2011. Coral biomineralization: From the gene to the environment. Journal of Experimental Marine Biology and Ecology 408: 58–78.
- Tewksbury JJ, Huey RB, Deutsch CA. 2008. Putting the heat on tropical animals. Science 320: 1296–1297.
- The Royal Society. 2005. Ocean Acidification Due to Increasing Atmospheric Carbon Dioxide. The Royal Society, London.
- Venn A, Tambutté E, Holcomb M, Laurent J, Allemand D, Tambutté S. 2013. Impact of seawater acidification on pH at the tissue-skeleton interface and calcification in reef corals. Proceedings of the National Academy of Sciences of the United States of America 110: 1634–1639.
- Venn A, Tambutté E, Holcomb M, Allemand D, Tambutté S. 2011. Live tissue imaging shows reef corals elevate pH under their calcifying tissue relative to seawater. PloS ONE 6: e20013.
- Verkhratsky A, Parpura V. 2014. Store-operated calcium entry in neuroglia. Neuroscience Bulletin 30: 125–33.
- Veron JEN, Pichon M.1976. Scleractinia of Eastern Australia. Part I. Families Thamnasteriidae, Astrocoeniidae, Pocilloporidae. Australian Government Publishing Service, Canberra. 208.
- Veron JEN, Pichon M. 1980. Scleractinia of Eastern Australia, Part III. Australian Institute of Marine Science, Monograph Series 4. Canberra: Australian Government Publishing Service.
- Vidal-Dupiol J, Adjeroud M, Roger E, Foure L, Duval D, Mone Y, Ferrier-Pages C, Tambutté E, Tambutté S, Zoccola D, Allemand D, Mitta G. 2009. Coral bleaching under thermal stress: putative involvement of host/symbiont recognition mechanisms. BMC Physiology 9: 14.
- Vihtakari M, Hendriks I, Holding J, Renaud P, Duarte C, Havenhand J. 2013. Effects of Ocean Acidification and Warming on Sperm Activity and Early Life Stages of the Mediterranean Mussel (*Mytilus galloprovincialis*). Water 5: 1890–1915.

- Warner ME, Fitt WK, and Schmidt GW. 1999. Damage to photosystem II in symbiotic dinoflagellates: a determinant of coral bleaching, Proc. Nat. Acad. Sci. USA, 96: 8007–8012.
- Wooldridge SA. 2013. Breakdown of the coral-algae symbiosis: towards formalising a linkage between warm-water bleaching thresholds and the growth rate of the intracellular zooxanthellae. Biogeosciences 10: 1647–1658.
- Young SD. 1973. Collagen and other mesoglea protein from the coral *Lobophyllia corymbosa* (anthozoa, scleractinia). Int. J. Biochem. 4(22): 339–344.
- Zeebe RE. 2012. History of Seawater Carbonate Chemistry, Atmospheric CO₂, and Ocean Acidification. Annu. Rev. Earth Planet. Sci. 141–165.
- Zoccola D, Tambutté E, Sénégas-Balas F, Michiels JF, Failla JP, Jaubert J, Allemand D. 1999. Cloning of a calcium channel alpha1 subunit from the reef-building coral, *Stylophora pistillata*. Gene 227: 157–167.